The FEBS Journal

FEBS PRESS science publishing by scientists

The metagenome-derived esterase PET40 is highly promiscuous and hydrolyses polyethylene terephthalate (PET)

Hongli Zhang[1], Robert F. Dierkes[1], Pablo Perez-Garcia[1,2], Elisa Costanzi[3], Jonas Dittrich[4], Pablo A. Cea[4], Marno Gurschke[1], Violetta Applegate[3], Kristina Partus[1], Christel Schmeisser[1], Christopher Pfleger[4], Holger Gohlke[4,5], Sander H. J. Smits[3,6], Jennifer Chow[1] and Wolfgang R. Streit[1]

1 Department of Microbiology and Biotechnology, University of Hamburg, Germany
2 Molecular Microbiology, Institute for General Microbiology, Kiel University, Germany
3 Center for Structural Studies, Heinrich Heine University, Düsseldorf, Germany
4 Institute for Pharmaceutical and Medicinal Chemistry, Heinrich Heine University, Düsseldorf, Germany
5 Institute of Bio- and Geosciences (IBG-4: Bioinformatics), John von Neumann Institute for Computing and Jülich Supercomputing Centre, Forschungszentrum Jülich GmbH, Germany
6 Institute of Biochemistry, Heinrich Heine University, Düsseldorf, Germany

Keywords
HMM; hydrolases; metagenome; PET degradation; promiscuity

Correspondence
W. R. Streit, Department of Microbiology and Biotechnology, University of Hamburg, Ohnhorststr. 18, D-22609 Hamburg, Germany
Tel: +49 40 42816 463
E-mail: wolfgang.streit@uni-hamburg.de

Hongli Zhang and Robert F. Dierkes shared first authorship
Dedicated to Karl-Erich Jaeger for his pioneering contributions in the field of molecular enzyme technology

(Received 31 January 2023, revised 24 July 2023, accepted 7 August 2023)

doi:10.1111/febs.16924

Polyethylene terephthalate (PET) is a widely used synthetic polymer and known to contaminate marine and terrestrial ecosystems. Only few PET-active microorganisms and enzymes (PETases) are currently known, and it is debated whether degradation activity for PET originates from promiscuous enzymes with broad substrate spectra that primarily act on natural polymers or other bulky substrates, or whether microorganisms evolved their genetic makeup to accepting PET as a carbon source. Here, we present a predicted diene lactone hydrolase designated PET40, which acts on a broad spectrum of substrates, including PET. It is the first esterase with activity on PET from a GC-rich Gram-positive *Amycolatopsis* species belonging to the Pseudonocardiaceae (Actinobacteria). It is highly conserved within the genera *Amycolatopsis* and *Streptomyces*. PET40 was identified by sequence-based metagenome search using a PETase-specific hidden Markov model. Besides acting on PET, PET40 has a versatile substrate spectrum, hydrolyzing δ-lactones, β-lactam antibiotics, the polyester-polyurethane Impranil® DLN, and various *para*-nitrophenyl ester substrates. Molecular docking suggests that the PET degradative activity is likely a result of the promiscuity of PET40, as potential binding modes were found for substrates encompassing mono(2-hydroxyethyl) terephthalate, bis(2-hydroxyethyl) terephthalate, and a PET trimer. We also solved the crystal structure of the inactive PET40 variant S178A to 1.60 Å resolution. PET40 is active throughout a wide pH (pH 4–10) and temperature range (4–65 °C) and remarkably stable in the

Abbreviations
aa, amino acids; BHET, bis(2-hydroxyethyl) terephthalate; CalB, *Candida antarctica* lipase B; CEC, cefaclor; CFT, cefotiam; DTT, dithiothreitol; EDTA, ethylenediaminetetraacetic acid; EG, ethylene glycol; EPPS, *N*-(2-hydroxyethyl)piperazine-*N*′-(3-propanesulfonic acid); HEPES, hydroxyethyl)piperazine-1-ethanesulfonic acid; HMM, hidden Markov model; IPM, imipenem; isPETase, *Ideonella sakaiensis* PETase; LB, lysogeny broth; LCC, leaf compost cutinase; MA, cefamandole; MEZ, mezlocillin; MH, methyl hexanoate; MHET, mono(2-hydroxyethyl) terephthalate; PCL, polycaprolactone; PCL_3, polycaprolactone trimer; PEG, polyethylene glycol; PET, polyethylene terephthalate; PET_3, polyethylene terephthalate trimer; PMSF, phenylmethylsulfonyl fluoride; *p*NP, *para*-nitrophenyl; *p*NP-C10, 4-nitrophenyl decanoate; *p*NP-C12, 4-nitrophenyl dodecanoate; RMSD, root-mean-square deviation; TBT, tributyrin; TPA, terephthalic acid; UHPLC, ultra-high performance liquid chromatography; ZOI, zone of inhibition.

presence of 5% SDS, making it a promising enzyme as a starting point for further investigations and optimization approaches.

Introduction

Petroleum-based plastics are, in general, extremely stable and durable. The global use at a multimillion tons scale over 70 years and the lack of recycling and circular use concepts have resulted in unprecedented pollution in nearly all environments [1,2]. Microbial- and enzyme-driven plastics degradation have made enormous progress in the last years, and several reviews have summarized the current knowledge [3–7].

Currently, around 80 enzymes originating from four different bacterial phyla are biochemically characterized PET-active hydrolases (www.pazy.eu database search, accessed on 02.05.23; [8]) (Fig. 1). These enzymes comprise cutinases (EC3.1.1.74), lipases (EC3.1.1.3), and carboxylesterases (EC3.1.1.1) that can act on amorphous and low-crystalline PET. They hydrolyze ester bonds in the polymer yielding bis-(2-hydroxyethyl) terephthalate (BHET), mono-(2-hydroxyethyl) terephthalate (MHET), terephthalic acid (TPA), and ethylene glycol (EG). Some bacteria can hydrolyze MHET using an MHETase [9,10]. TPA can be degraded via cleavage of the aromatic ring structure using known aryl pathways [11,12]. While EG is often oxidized to glycolate before entering glyoxylate degradative pathways.

The best-studied enzymes are derived from the Gram-negative proteobacterium *Ideonella sakaiensis* 201-F6 [9] and from a leaf branch compost metagenome [15]. The latter is a designated leaf and branch compost cutinase (LCC) and is phylogenetically affiliated with the Gram-positive genus *Thermobifida* [15]. This genus together with the closely related genera *Thermomonspora* and *Saccharomonospora* are phylogenetically grouped within Actinobacteria and have been a rich source for PET hydrolases [16–22] (Fig. 1). Also, it has been shown that the Gram-negative genus *Pseudomonas* (Proteobacteria) harbors a diverse set of PET-active enzymes, listed in the PAZy database (www.pazy.eu). Among them are PpCutA from *P. pseudoalcaligenes*, PpelaLip derived from *P. pelagia* and PE-H from *P. aestusnigri* [23–25]. Additionally, we recently reported on PET-degrading enzymes found in the Bacteroidetes phylum [26]. Altogether, these studies have significantly advanced our knowledge of the structural and biochemical processes affiliated with PET hydrolysis [10,27,28]. Furthermore, *Candida antarctica* lipase B (CalB), *Fusarium solani* FsC, and *Humicola insolens* HiC were affiliated with PET degradation as part of promiscuous enzyme activities [29]. Since it is well-known that some esterases are highly

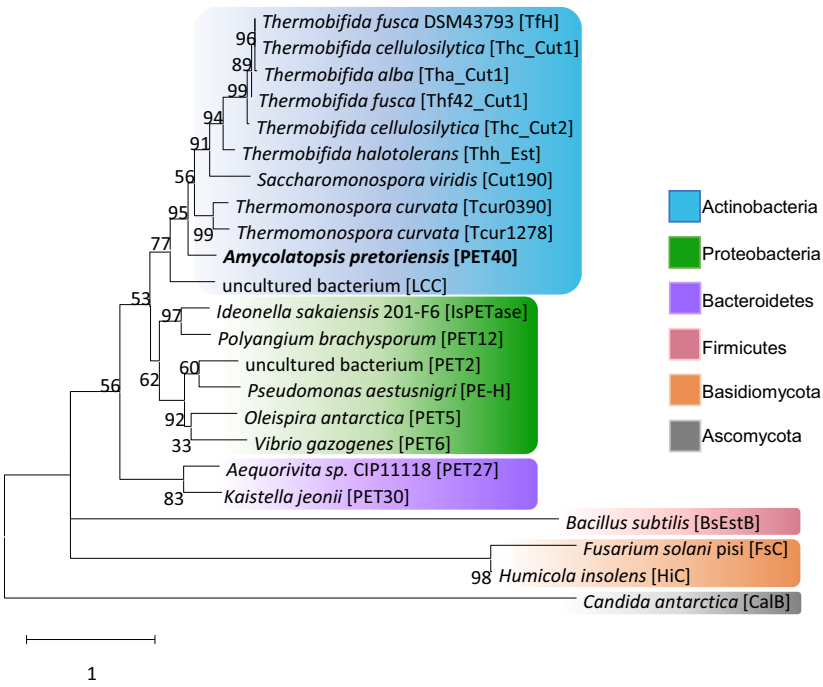

Fig. 1. PET40 shares sequence similarities with other actinobacterial PETases and LCC. The unrooted phylogenetic tree is based on amino acid sequence homologies. Overall, a selection of 23 enzymes was included in this alignment. The structural alignment was calculated with T-COFFEE EXPRESSO [13]. The tree was constructed by a Maximum Likelihood method using MEGAX [14] with 1000 bootstraps. The bootstrap values are indicated as percentages at the branches. GenBank entries of the sequences used are listed in Table 1 and on www.pazy.eu. The phylogenetic groups are highlighted with distinct colors, as shown in the legend.

Table 1. Functionally verified and known PET-active enzymes in the phylum of the Actinobacteria.

Name	GenBank accession	Phylogenetic affiliation	Reference	aa sequence identity with PET40 (%)
PET40	WAU86704.1	*Amycolatopsis* sp.	This work	100.00
Cut190	BAO42836.1	*Saccharomonospora viridis* AHK190	[19]	65.40
LCC	AEV21261.1	Uncultured bacterium	[15]	58.94
Tcur0390	WP_012850775.1	*Thermomonospora curvata* DSM43183	[38]	68.34
Tcur1278	WP_012851645.1	*Thermomonospora curvata* DSM43183	[20]	69.14
TfH	WP_011291330.1	*Thermobifida fusca* DSM43793	[21]	63.70
Thc_Cut1	ADV92526.1	*Thermobifida cellulosilytica* DSM44535	[22]	63.60
Thc_Cut2	ADV92527.1	*Thermobifida cellulosilytica* DSM44535		62.84
Thf42_Cut1	ADV92528.1	*Thermobifida fusca* DSM44342		62.45
Tha_Cut1	ADV92525.1	*Thermobifida alba* DSM43185	[16]	62.45
Thh_Est	AFA45122.1	*Thermobifida halotolerans* DSM44931		68.97

promiscuous [30,31] and the turnover rates of wild-type enzymes on PET are low to moderate, we assume that PETases are in general rather promiscuous enzymes and PET is not the native substrate. Our understanding of the origin, evolution, and role of PET-active enzymes in the environment is still very poor. These challenges can only be met by mining biodiversity for novel enzymes and analyzing and comparing their structural, phylogenetic, and kinetic characteristics.

Within this framework, and to further enrich the biodiversity of known PET-active enzymes, we have searched for new PET-active enzymes. Therefore, we used a previously published hidden Markov model (HMM) search algorithm to mine global genomes and metagenomes [32,33]. We identified a single novel esterase, designated PET40, that is distinct from previously identified enzymes in the Actinobacteria. Intriguingly, PET40 is highly conserved within the genera of *Amycolatopsis* and *Streptomyces*. The enzyme is highly active on a wide range of different substrates, including PET, and has remarkably good activity on *para*-nitrophenyl (*p*NP)-esters even at temperatures as low as 4 °C. While it is already known that some predicted diene lactone hydrolases can degrade PET [34], this study is one of the first that highlights substrate promiscuity aspects of a PET-active esterase by delivering experimental and structural evidence.

Results

Profile hidden Markov model search identifies the novel actinobacterial PET-active esterase PET40

Previous research has shown that bacterial PET esterases occur in four bacterial phyla (Fig. 1). Most of the verified PET-active enzymes have been identified in the phylum of the *Actinomycetes* with 33 biochemically characterized enzymes (www.pazy.eu, accessed on 02.05.23). Since hitherto only in the three closely related genera *Thermobifida*, *Thermomonspora*, and *Saccharomonospora* active PETases had been identified, we wondered whether other GC-rich Gram-positive Actinobacterial genera code for PET-active enzymes. To address this question, we performed global database searches on publicly available bacterial genomes and metagenomes from the NCBI GenBank [35]. and IMG database [36]. combined with a previously published HMM-based search approach [32,33]. Among others, this search identified a potential diene lactone hydrolase in a soil metagenome affiliated with the Gram-positive genus *Amycolatopsis* from a biochar metagenome (Table 1) [37]. We designated this putative PETase PET40. A phylogenetic analysis of the deduced amino acid sequence implied that the predicted enzyme was phylogenetically related to known actinobacterial sequences, but not affiliated with any of the three genera *Thermobifida*, *Thermomonospora*, and *Saccharomonospora*. The amino acid alignment shows that the amino acid sequence similarity of PET40 ranged from 58.9% to 69.1% compared with the known high-GC bacterial PETases listed in Table 1. Based on this observation, we performed additional BLASTP searches using the PET40-deduced amino acid sequence. Interestingly, the enzyme is relatively conserved within the genus of *Amycolatopsis*. It is present in 21 of the 68 *Amycolatopsis* genomes deposited in GenBank with *E*-values ranging from $7e^{-172}$ to $1e^{-149}$ and the lowest identity of 93% (94% coverage). Using an arbitrary identity cutoff of 80%, we found the protein sequence in 73 of the 564 *Streptomyces* genomes from the NCBI genome database with the highest *E*-value of $7e^{-144}$ (81% identity at 95% query coverage). These data imply that the protein is widely distributed within these two genera and may have been

acquired via horizontal gene transfer within these GC-rich Gram-positive microorganisms.

Recombinant PET40 hydrolyzes TBT, PCL, BHET, the ester-based polyurethane Impranil DLN, and PET

To verify our bioinformatic analysis, we expressed PET40 in *Escherichia coli* for functional characterization. For this, the candidate gene was synthesized, cloned into the expression vector pET21a(+) (Biomatik, Wilmington, DA, USA), and transformed in *E. coli* BL21 (DE3). Initial tests using recombinant purified proteins and agar plates containing tributyrin (TBT) indicated the PET40-gene codes for an active esterase (Fig. 2A). PET40 was able to hydrolyze BHET (Fig. 2A), which is a monomeric constituent of PET used as a screening substrate to indicate possible activity on PET. Activity on polycaprolactone (PCL), a polyester model-substrate, could also be shown (Fig. 2A). The hydrolysis of these model substrates also indicates possible activity on the polymeric and more complex PET. Additionally, we observed that PET40 was able to cleave Impranil® DLN, which is an aliphatic polyester polyurethane. After an incubation for 20 min at 40 °C with 5 μg PET40 (250 μL reaction volume), a release of 790 ± 21 μM of H^+ was detectable using phenol red as the indicator (Fig. 2B). Ultra-high-performance liquid chromatography (UHPLC) analyses confirmed the release of hydrolysis products such as TPA from semicrystalline (> 40% crystallinity) PET powder after incubation with PET40 (Fig. 2C).

PET40 (0.1 mg·mL^{-1} enzyme in 200 μL corresponding to 3.54 μM) was incubated together with 5 mg PET powder for 72 h at 40 °C. After the incubation, a concentration of aromatic degradation products TPA, MHET, and BHET of 50.41 ± 10.21 μM was measured in the reaction supernatant corresponding to a relative amount of 0.17 ± 0.03 μmol TPA-EG unit

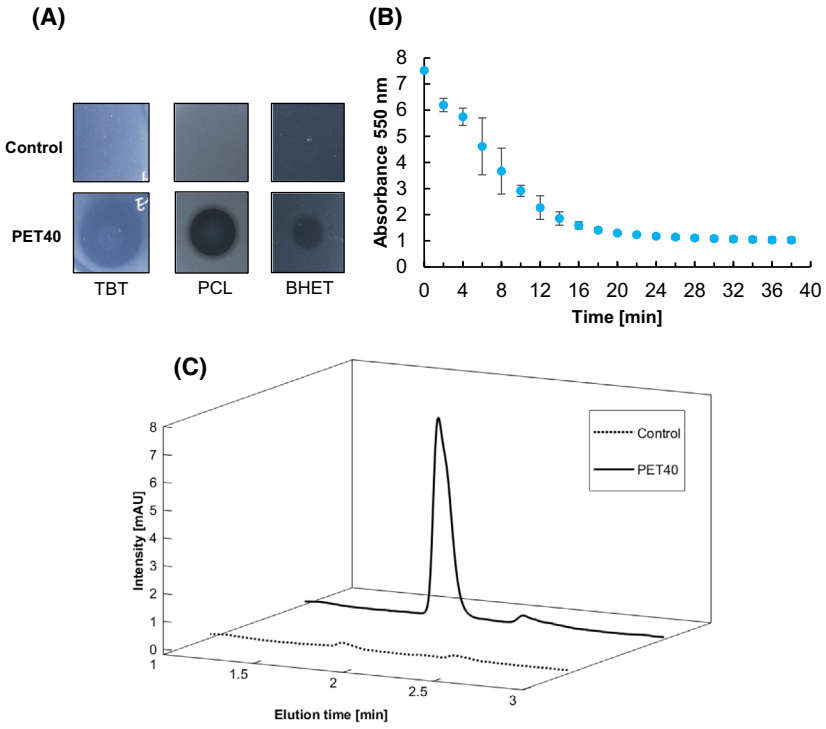

Fig. 2. PET40 hydrolyses various esters, including PET. (A) Activities of PET40 on TBT, PCL, and BHET using agar plates. 10 μL containing 10–100 μg of purified enzyme were applied to agar plates containing either 33.08 mM TBT, 4.38 mM PCL, or 5 mM BHET. Halos were observed after 12 h. Control indicates plates with 10 μL enzyme-free buffer. (B) Activity on Impranil® DLN was assessed using phenol red as pH indicator. Decreasing values of absorbance at 550 nm revealed the breakdown of Impranil® DLN by PET40. Error bars represent standard deviation (SD) values of $n = 3$ measurements. (C) UHPLC profile of PET40 reaction supernatant after incubation on PET powder for 72 h showing the release of TPA (elution time: 1.7 min). 0.1 mg·mL^{-1} of recombinant and purified enzyme were applied to 5 mg of PET powder in a reaction volume of 200 μL and incubated over 72 h at 40 °C. The chromatograms are representative measurements, which were repeated in separate experiments at least three times. A control of an equal amount of PET powder was incubated at the same conditions without added enzyme to rule out non-enzymatic TPA release.

released from the polymer per mg of enzyme per day (Table 2). For comparison, we assessed the activity of PET40 to self-produced recombinant IsPETase and LCC under equal conditions at suitable temperatures. Here, IsPETase released at 30 °C 4.33 ± 0.56 $\mu mol_{TPA\text{-}EG} \cdot mg_{enzyme}^{-1} \cdot day^{-1}$ and LCC at 50 °C released 12.78 ± 1.44 $\mu mol_{TPA\text{-}EG} \cdot mg_{enzyme}^{-1} \cdot day^{-1}$.

Even though activity on PET can be detected for PET40 through HPLC measurements, the overall PET degradation takes place at a low rate with a substrate conversions below 0.1% in the incubations specified above. The low activity compared with IsPETase or LCC may be related to a single amino acid substitution in the predicted substrate binding pocket of PET40 (Table 3). Notably, IsPETase and LCC carry a Tyr-Met-Trp motif in their binding sites. PET40, however, carries a Phe-Met-Trp motif (Fig. 3, Table 3).

Promiscuity assays using esterase, lactonase, and β-lactamase substrates

Due to the rather recent occurrence of PET in the environment, it is unlikely that the primary substrate of a natural esterase is PET and degradation of the polymer is often only a side activity, as esterases are known to be promiscuous enzymes [30,31]. This also justifies the low turnover rates of PET40 on PET. Therefore, we further characterized PET40 on *p*NP esters, lactones, and β-lactams. Furthermore, we tested the effect of metal ions on PET40 activity.

Para-nitrophenyl-esters are commonly used substrates for the biochemical characterization of carboxylesterases. Using *p*NP esters with a C-chain length ranging from 4 to 18 (*p*NP C4-C18), PET40 showed activities on all substrates, with higher activities observed on *p*NP-esters with acyl chain lengths between C6 and C14 (Fig. 4A). Significantly lower activities were measured with shorter (C4) and longer (C16–18) C-chain lengths. The kinetic parameters of PET40, determined according to Michaelis–Menten for *p*NP-C12 at 30 °C and pH 8, are v_{max} = 0.86 nmol·min^{-1}, k_{cat} = 8.26 s^{-1}, K_m = 0.73 mM, and k_{cat}/K_m value of 1.14 × 10^4 M^{-1}·s^{-1}.

Table 2. TPA-EG units (μM) released from PET by PET40 in comparison with *Is*PETase and LCC. The recombinant and purified enzymes were incubated at a concentration of 0.1 mg·mL^{-1} for a time period of 72 h at 40 °C (PET40), 50 °C (LCC) and 30 °C (*Is*PETase), respectively. For the tests, 5 mg of PET powder (as specified in Materials and methods) were employed. Incubations were carried out in a reaction volume of 200 μL. Data are mean values with standard deviations derived from three measurements per sample.

Enzyme	Phylum	Released $\mu mol_{TPA\text{-}EG} \cdot mg_{enzyme}^{-1} \cdot day^{-1}$
PET40	Actinobacteria	0.17 ± 0.03
LCC		12.78 ± 1.44
IsPETase	Proteobacteria	4.33 ± 0.57

Using 1 mM *p*NP-C12 as substrate, PET40 revealed a remarkably broad temperature range. PET40 was most active at pH 8.0 when tested in 0.1 M potassium phosphate buffer with 1 mM of substrate at the temperature optimum of 40 °C. Surprisingly, at 4 °C, the enzyme still showed a relative activity of 59% compared with the activity at optimal conditions (Fig. 4A). At 40 °C, PET40 is also active over a broad pH range (pH 5–10), for which more than 75% residual activity was observed. To assess the enzyme's thermostability, it was incubated at 50 °C and 60 °C for 2 h, after which the enzyme only showed 11% and 5% residual activity, respectively, compared with the control without incubation (data not shown). At 50 °C, PET40 has a half-life time of 30 min (Fig. 4B). Nano differential scanning fluorimetry (NanoDSF) measurements indicated a T_m of 54.56 ± 0.24 °C of the protein. To further characterize the effects of metal ions, possibly conveying activity through increased stability to the enzyme, Ca^{2+}, Co^{2+}, Cu^{2+}, Fe^{3+}, Mg^{2+}, Mn^{2+}, Ni^{2+}, or Zn^{2+}, were added to the assays at 1 and 10 mM. The activity was measured with *p*NP-C12 and compared with a metal-free control. The activity of PET40 slightly decreased at a 10 mM concentration for most of these ions and was mostly unaffected at the 1 mM concentration (Fig. 4A). Therefore, we conclude that the enzyme does not need metal ions for its activity. To probe PET40's tolerance against chelating agents and inhibitors, we tested the influences of ethylenediaminetetraacetic acid (EDTA), dithiothreitol (DTT), or phenylmethylsulfonyl fluoride (PMSF) in concentrations of 1 and 10 mM. The presence of EDTA, DTT, and PMSF resulted in < 20% reduction in activity which, regarding EDTA, is also in line with the findings about the unaffectability through metal ions. Finally, we tested the sensitivity of PET40 toward detergents. A concentration of 5% (v/v) of the detergents Tween 80 and Triton X-100 lead to a decrease of 80% and 32%, respectively. SDS at the same concentrations had no negative impact on the enzyme's activity (Fig. 4A). Thus, PET40 has a relatively high stability against denaturing agents.

Lactonase activity of PET40 was further investigated in a phenol red assay, where the hydrolysis on δ-dodecalactone, γ-dodecalactone, δ-octalactone, and γ-caprolactone was detected due to the release of protons. These lactones differ in their chain length and ring structure. PET 40 showed the highest activity on δ-octalactone (0.43 U·mg^{-1}). While δ-dodecalactone

Table 3. Conserved motifs and structural features identified in PET40 and other PETases. The *Ideonella sakaiensis* PETase (IsPETase, PDB: 6EQE; [9,39]), LCC (4EB0; [40]), PET2 [32], the Bacteroidetal enzyme PET27 and PET30 were included for benchmarking purposes. PorC, Por secretion system C-terminal sorting domain; SP, signal peptide; β, β-sheet; –, none.

						C-terminus	
Predicted PETase	SP cleavage site	Catalytic triad	Substrate binding site	Disulfide bonds[a]	N-terminal SP	Secondary structure	Conserved domain
IsPETase	27–28	Asp-His-Ser	Tyr-Met-Trp	2×	Sec/SPI	–	–
LCC	21–22	Asp-His-Ser	Tyr-Met-Trp	1×	Sec/SPI	–	–
PET2	27–28	Asp-His-Ser	Tyr-Met-Trp	2×	Sec/SPI	–	–
PET27	23–24	Asp-His-Ser	Phe-Met-Trp	1×	Sec/SPI	7xβ	PorC
PET30	23–24	Asp-His-Ser	Phe-Met-Tyr	1×	Sec/SPI	7xβ	PorC
PET40	47–48	Asp-His-Ser	Phe-Met-Trp	2×	Sec/SPI	–	–

[a]Verified and predicted disulfide bonds.

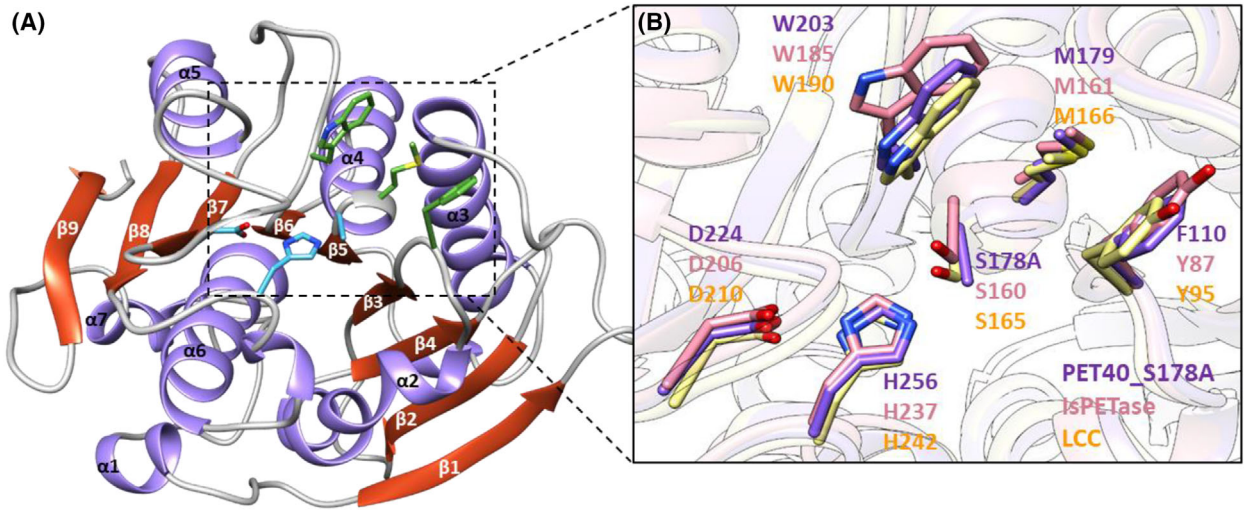

Fig. 3. Crystal structure of PET40_S178A and alignment with known IsPETase and LCC. (A) The structure of PET40_S178A was solved by X-ray crystallography. Cartoon representation showing the secondary structure elements and the active site (box). The catalytically active amino acids are colored in blue, and the substrate binding site is colored green. In the solved crystal structure the catalytic serine was mutated to alanine. (B) The residues of the active site of PET40_S178A (purple), IsPETase (pink; PDB code 6EQE), and LCC (yellow; PDB code 4EB0) were overlaid by CHIMERA 1.13.1. The amino acids related to the catalytic activity are labeled. The catalytic triad is conserved within all three structures (Ser; Asp; His), but PET40 has Phe instead of Tyr at the first position of the substrate binding site. Structures were generated using UCSF CHIMERA version 1.13.1 [41].

was cleaved rather quickly (0.22 $U \cdot mg^{-1}$), γ-dodecalactone was not (0.06 $U \cdot mg^{-1}$). The hydrolysis rate of γ-caprolactone (0.02 $U \cdot mg^{-1}$) was similar to that of γ-dodecalactone.

The activity of PET40 on different β-lactams (Fig. 5A) was tested in a standard disk diffusion assay on agar plates. The commercially available disks used in this assay contained indicated amounts of antibiotic compounds (Fig. 5B). The zone of inhibition (ZOI) of bacterial growth around these disks was evaluated after incubation of the disks with PET40. Susceptible *E. coli* DH5α cells were cultivated together with the pre-incubated disks on lysogeny broth (LB)-agar plates. The inhibition zones are smaller or even not present when the antibiotics have been inactivated. The results were compared with control disks incubated without enzyme. PET40 was able to reduce the inhibitory effect of mezlocillin 30 μg (MEZ 30, ureidopenicillin group), cefamandole 30 μg (MA 30), and cefaclor 30 μg (CEC 30, cephalosporin 2nd generation) completely, and cefotiam 30 μg (CFT 30, cephalosporin 3rd generation) to 95.9%. Interestingly, PET40 did not reduce the inhibitory effect of imipenem 10 μg (IPM 10), which belongs to the carbapenem group (Fig. 5B) and is an antibiotic of last resort.

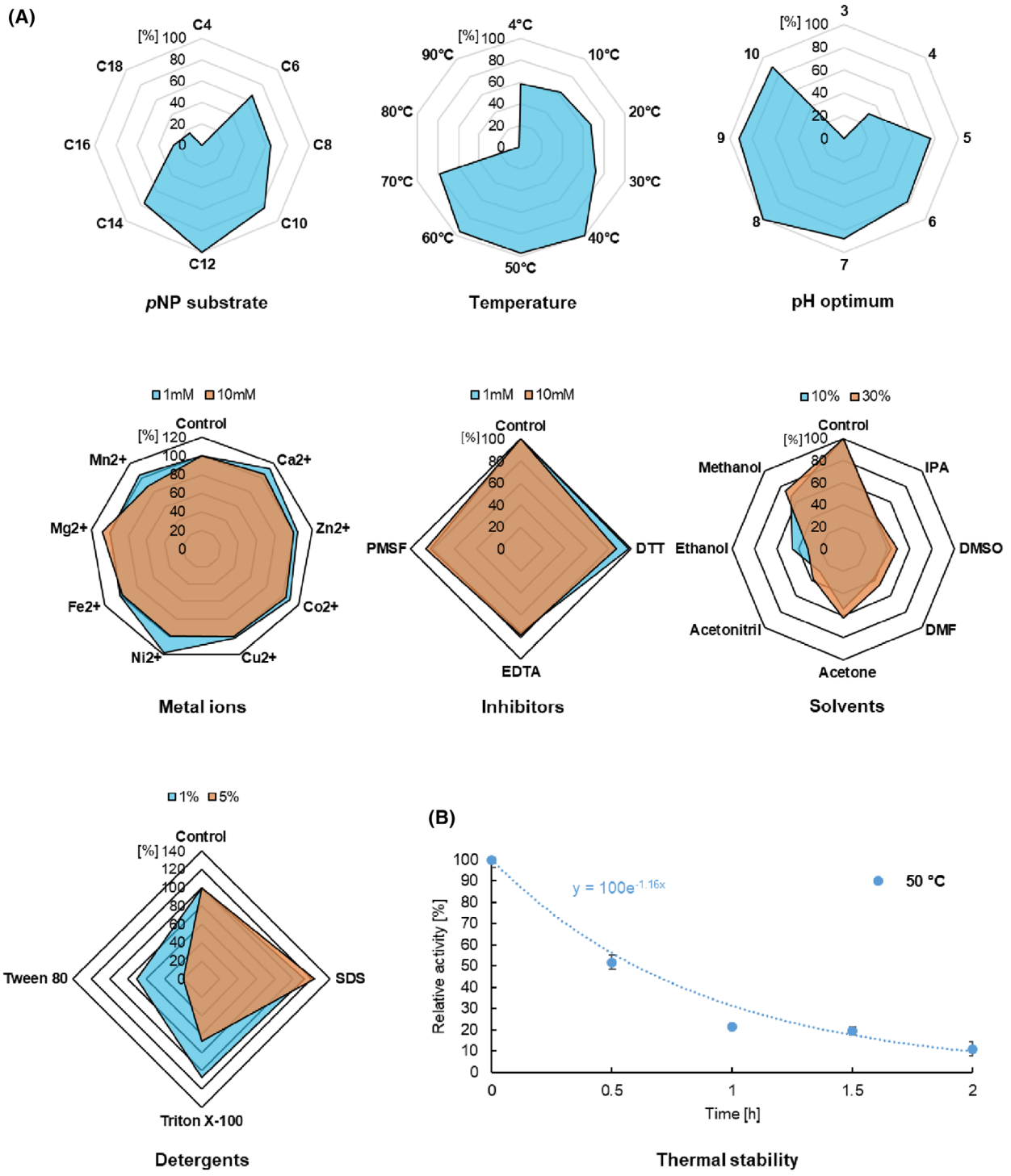

Fig. 4. Biochemical characterization of PET40 using C4-C18 *p*NP esters. (A) Net diagrams depicting the substrate preference, temperature optimum, pH optimum as well as the influence of different metal ions, inhibitory agents, solvents and detergents on the activity of PET40. In all cases, standard deviations were lower than 7%. (B) Graph showing the thermal stability of PET40 at 50 °C over 2 h with an exponential fit (R^2 = 0.94). Data represent mean values of three replicates (n = 3). Error bars represent standard deviations (SD). During all incubations, 0.25 μg enzyme were incubated for 10 min in 200 μL reaction volume under the different tested conditions. All tests besides substrate preferences were carried out with *p*NP-C12.

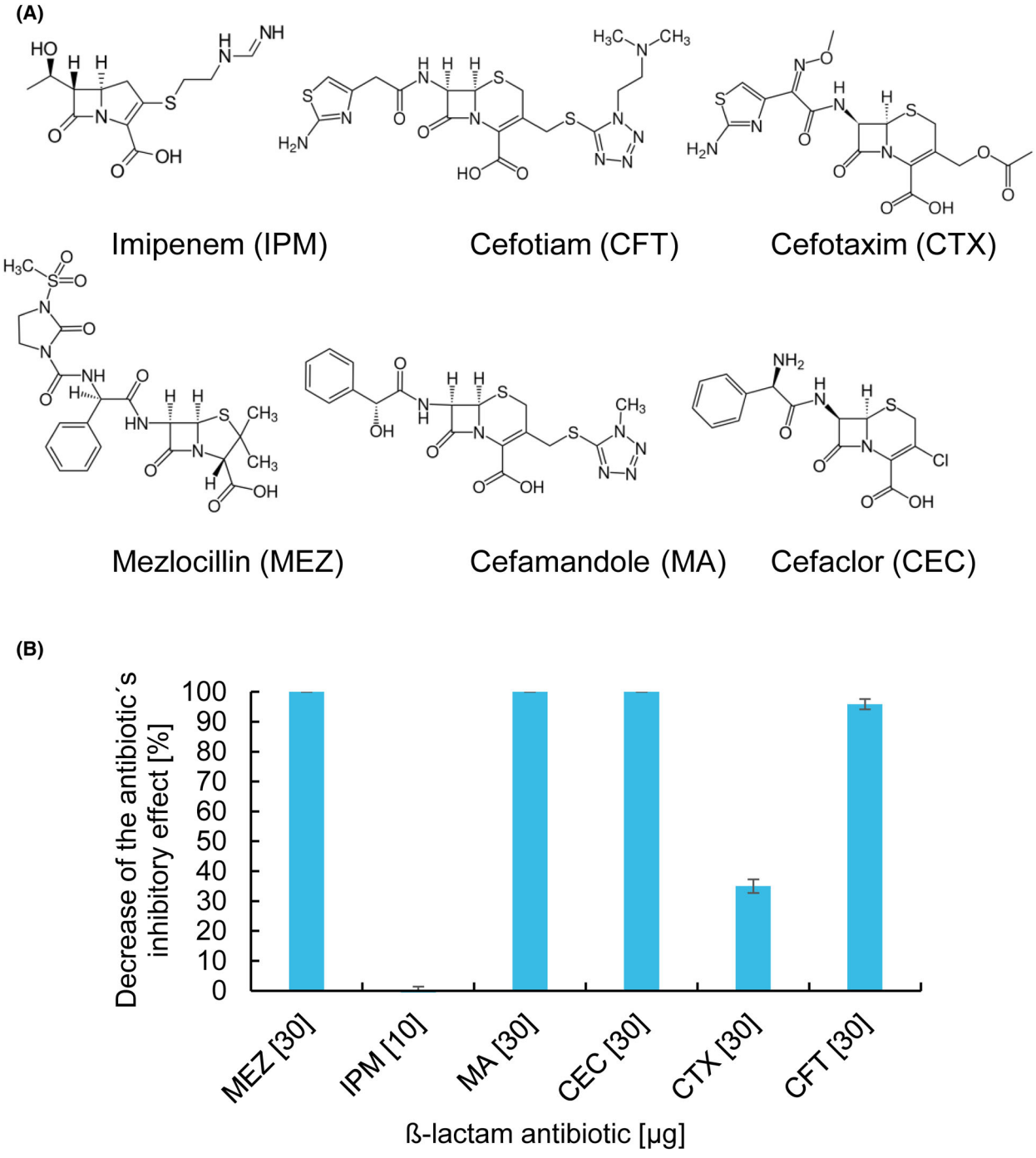

Fig. 5. The promiscuous PET40 degrades β-lactam antibiotics. (A) Overview and structures of β-lactam antibiotics used in degradation tests. (B) Inhibitory effect of PET40 on different β-lactam- antibiotics. Antibiotic assay disks (total amounts as stated in square brackets) were incubated over 17 h in 20 µL potassium phosphate buffer (0.1 M, pH 8) containing 1 mg·mL^{-1} purified PET40. After incubation the plates were laid on agar plates on which susceptible *Escherichia coli* DH5α cells had been plated out. Disks that were incubated only with buffer served as controls. The ZOI was determined by measuring the halo around the disks. The inhibitory effect of MEZ 30, MA 30, and CEC 30 was diminished completely by PET40 and in the case of CFT 30 to more than 95%. Abbreviations for the used antibiotics are as follows: Mezlocillin 30 µg (MEZ 30), imipenem 10 µg (IPM 10), cefamandole 30 µg (MA 30), cefaclor 30 µg (CEC 30), cefotaxim 30 µg (CTX 30) and cefotiam 30 µg (CFT 30). Error bars represent standard deviations (SD) of nine replicates (n = 9).

In summary, the data show that PET40 is a promiscuous, cofactor-independent, mesophilic enzyme that is able to act on the polymers PET, Impranil and PCL, as well as *p*NP-esters, lactones and β-lactams. Its temperature optimum lies at 40 °C. PET40 retained more than 50% relative activity at temperatures as low as 4 °C (Fig. 4). The enzyme was rapidly deactivated when incubated at temperatures above 50 °C.

Amino acid sequence and structural analyses identify unique traits of PET40

Amino acid sequence analysis revealed that PET40 contained N-terminal signal domains for protein transport as predicted with SignalP 6.0 [42]. The predicted cleavage site was located between amino acid (aa) positions 47 and 48 with the signal peptide using the standard secretory signal peptides (likelihood of 0.73) (Table 3). Further sequence analysis identified a G-x-S-x-G motif typical for α/β serine hydrolases between aa positions 176 and 180 [43]. To investigate the structural traits of this promiscuous enzyme, PET40_S178A, an inactive variant of PET40, was generated by restriction-free cloning. We obtained well-diffracting crystals of PET40_S178A reaching a resolution of 1.60 Å. The crystal was packed in space group $P2_1$, with two molecules in the asymmetric unit. As confirmed by PISA [44], the biological unit is a monomer, and the overall root-mean-square deviation (RMSD) between the two chains present in the asymmetric unit is 0.161 Å, making them virtually identical. We were able to unambiguously model the protein chains in the electron density from residues 48 and 49 for chains A and B, respectively, to residue 309. A portion of the His-tag was also visible in the electronic density for both chains, mediating crystal contacts with symmetric molecules. The final model was refined to R_{work}/R_{free} values of 14.59/17.90. All data collection and refinement statistics are reported in Materials and methods section.

The crystal structure shows that PET40 shares the typical fold of α/β serine hydrolases, composed by a central twisted β-sheet surrounded by α-helices. For PET40, the β-sheet consists of nine β-strands and is surrounded by seven α-helices (Fig. 3). The RMSD between PET40 and IsPETase (PDB ID: 6EQE) is 0.570 Å, while it is 0.561 Å with LCC, which confirms the high structural similarity with known PETases. As previously shown for other Type II PET-degrading enzymes, a disulfide bond is present in PET40 between C289 and C305 [26,27]. PET40 possesses a catalytic triad consisting of the residues Asp-His-Ser, in a spatial arrangement highly similar to IsPETase and LCC (Fig. 3). The substrate binding site contains the aa residues Phe-Met-Trp. The latter differs from the known IsPETase and LCC binding sites in which a Tyr was reported in the first position (Fig. 3, Table 3). It is, however, in consonance with the bacteroidetal PETase PET27 [26] and Cut190 [45].

Binding mode prediction via molecular docking

To obtain insights into the potential binding modes of the diverse substrates in the active site of PET40, we performed molecular docking using a combination of AutoDock3 [46] as a docking engine and DrugScore^{2018} [47,48] as an objective function as done previously [24,49,50]. We focused on the ester substrates investigated experimentally in this study for the docking, that is mono(2-hydroxyethyl) terephthalate (MHET), bis(2-hydroxyethyl) terephthalate (BHET), PET trimer (PET_3), methyl hexanoate (MH), polycaprolactone trimer (PCL_3), propane-1,2,3-triyl tributanoate (tributyrin, TBT), 4-nitrophenyl decanoate (*p*NP-C10), and 4-nitrophenyl dodecanoate (*p*NP-C12). We performed 100 independent docking runs for each substrate, which were subsequently clustered into distinct docking poses based on structural similarity (RMSD cut-off < 2 Å).

For all substrates, except *p*NP-C10/12, the binding pose identified as best based on the binding score (Table 4), shows a conformation in which the reactive carbonyl carbon of the ester moiety is close to the Ser of the catalytic triad (Fig. 6). For *p*NP-C10/12, the best-scored binding pose involves interactions of the nitro moiety with the catalytic triad. The docking pose from the largest cluster only scored marginally worse (< 2% compared with the best-scored solution)

Table 4. Docking scores of the representatives of up to the three best-scored clusters for all docking substrates.

	Lowest docked energy[a]		
Substrate	Cluster 1	Cluster 2	Cluster 3
MHET	**−8.52**	−8.44	−8.37
BHET	**−9.84**	−9.62	−9.53
PET_3	**−16.58**	−15.61	−15.58
MH	**−6.33**	−5.51	n.a.[b]
*p*NP-C10	−11.94	−11.50	**−11.32**
*p*NP-C12	−12.75	**−12.28**	−12.11
PCL_3	**−12.72**	−12.28	−12.04
TBT	**−11.20**	−10.66	−10.60

[a]Sum of the estimated intermolecular energy and internal energy of the ligand in kcal·mol^{-1}. The energy of the pose depicted in Fig. 6 is marked in bold.; [b]Not available as only two clusters were obtained.

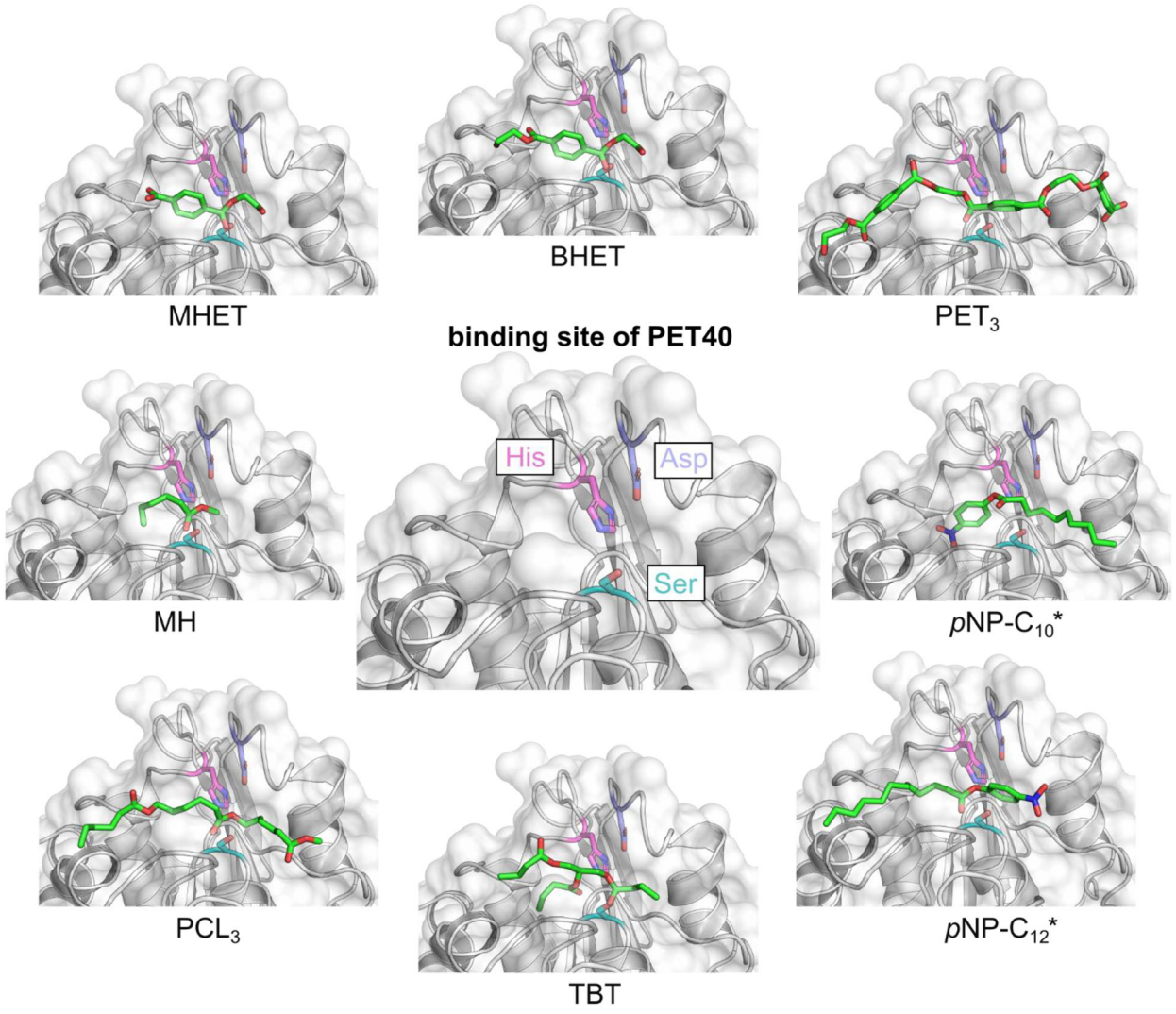

Fig. 6. PET40 has an active site cavity that can accommodate a large variety of substrates. Docking poses identified as best for mono(2-hydroxyethyl) terephthalate (MHET), bis(2-hydroxyethyl) terephthalate (BHET), PET trimer (PET_3), methyl hexanoate (MH), polycaprolactone trimer (PCL_3), propane-1,2,3-triyl tributanoate (tributyrin, TBT) in the binding site of PET40 (depicted without substrate in the center). *For 4-nitrophenyl decanoate (*p*NP-C10) and 4-nitrophenyl dodecanoate (*p*NP-C12), binding modes from the largest cluster were chosen rather than those with the lowest energy. Structures were generated using PYMOL [54].

and captures the key interactions of the ester carbonyl carbon with the serine. Thus, we consider this docking pose more relevant for the reaction of *p*NP-esters in PET40. The aliphatic chains of pNP-C10 or 12 point in opposite directions. However, it is not uncommon that a ligand or ligands with minor structural changes can bind to a protein in different poses [51,52], and the determined binding pose can even be impacted by the method used for structure elucidation [53].

For small ligands with a limited number of degrees of freedom, such as MH and MHET, our docking converges to two and three binding poses, respectively. However, for more complex ligands with a high number of degrees of freedom, such as PET_3 and PCL_3, we obtain a high number of clusters that mainly differ in the conformation at the end of the oligomer chain. However, the orientation of the reactive carbonyl carbon atom to the hydroxyl group oxygen of the serine is similar in most cases. Therefore, we calculated the minimum distance between the serine hydroxyl group oxygen and the reactive carbonyl carbon of each substrate for all docking runs (Fig. 7) to evaluate whether the substrate is close enough to the catalytic triad for a reaction to take place. This distance is < 5 Å for all substrates for the majority (> 55% for all cases, up to

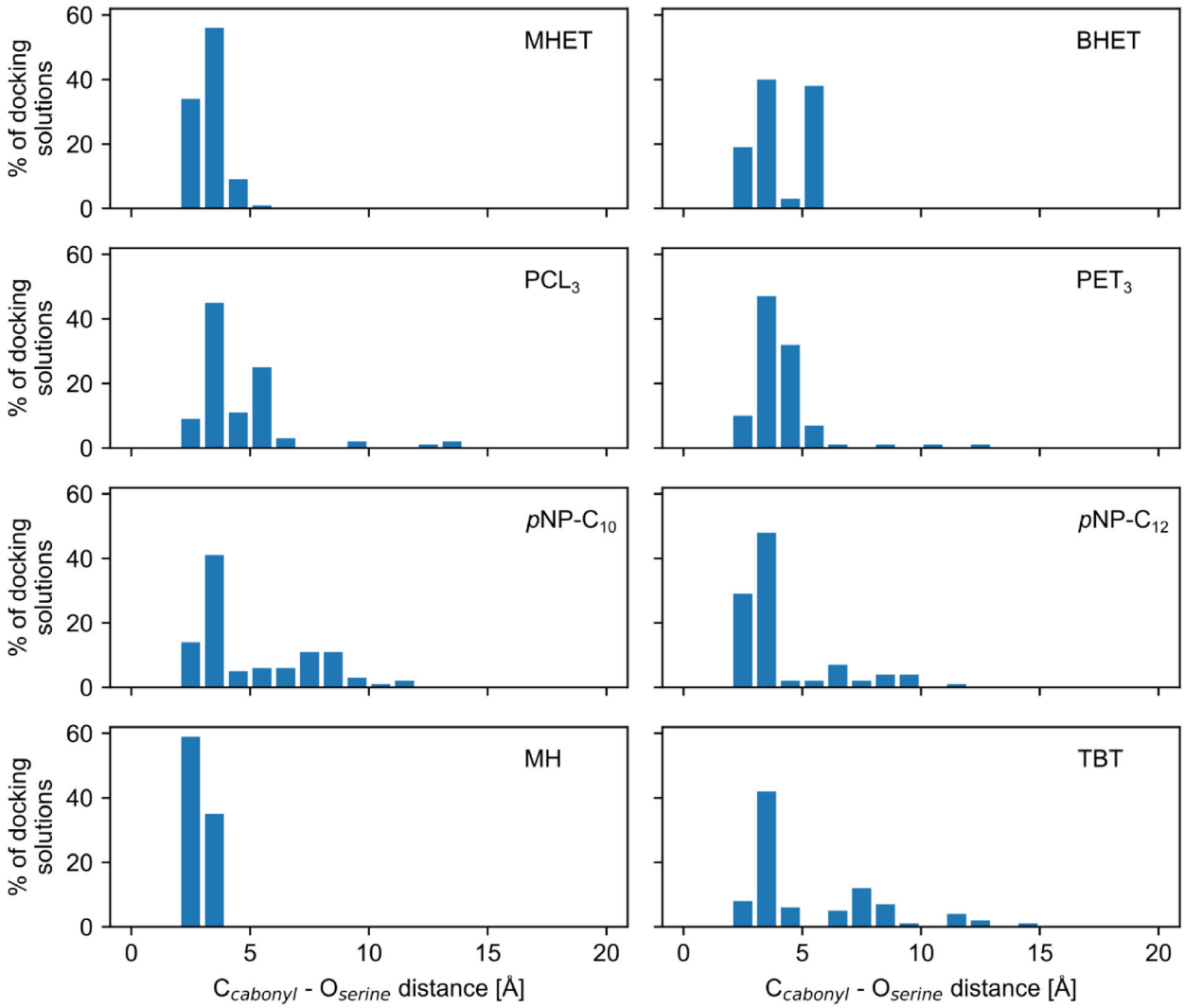

Fig. 7. Histograms of the minimum distance between the serine hydroxy group oxygen of PET40 and the electrophilic carbonyl carbon of the substrate for all obtained docking solutions. The following substrates were docked: mono(2-hydroxyethyl) terephthalate (MHET), bis(2-hydroxyethyl) terephthalate (BHET), a polycaprolactone trimer (PCL_3), a PET trimer (PET_3), 4-nitrophenyl decanoate (pNP C10), 4-nitrophenyl dodecanoate (pNP-C12), methyl hexanoate (MH), and propane-1,2,3-triyl tributanoate (tributyrin, TBT).

95% for MH) of the docking solutions (Fig. 7). Thus, our docking approach yields binding poses in line with the geometry required for a reaction for all substrates, despite the high number of degrees of freedom of some of the investigated substrates.

Overall, we find that relatively small substrates such as the polymeric building blocks MHET, BHET, and MH, but also bulky ligands such as TBT and the *p*NP-esters are well-accommodated by the active site of PET40 and can come close to the Ser of the catalytic triad with their electrophilic carbon. The binding site is located at the protein surface, facilitating the access of small and bulky substrates. Even for such binding sites, using an appropriate docking engine and objective function as done here can yield good binding modes with only a moderate drop-off compared with docking to "classical" binding sites [55]. Moreover, more complex substrates such as PET_3 and PCL_3 are also well-docked into the catalytic site, again pointing the reactive ester moiety toward the catalytic Ser. These results mirror the activity analyses on these substrates, which all were cleaved by PET40.

In the case of the β-lactam antibiotics, the binding poses generated by AutoDock3-DrugScore[2018] did not yield catalytically viable complexes. For this reason, we employed GLIDE as an alternative to generate putative binding poses. We docked the six experimentally tested antibiotics and assessed the distance between the serine

hydroxyl group of PET40 and the carbonyl carbon of the lactam group, as well as the angle described by the serine hydroxyl group, the carbonyl carbon, and the carbon opposite to it in the lactam ring, and compared the obtained values with the values of a crystallized Michaelis–Menten complex of a serine β-lactamase (Fig. 8A). The results show that for the five degraded antibiotics, we identified at least one docking solution with pairs of distance/angle values close to the values observed in the crystal structure (Fig. 8B). However, for imipenem, the only nondegraded antibiotic, no catalytically viable docking solution was identified. In the predicted binding poses of the five degraded antibiotics, the β-lactam ring is positioned in a consistent orientation within the active site (Fig. 9). Overall, the docking results can provide a structure-based explanation for the observations in the disk diffusion assays.

Discussion

Today's major global plastic pollution in all environments makes the study of plastic-degrading microorganisms and enzymes compulsory. Still, the number of functionally verified microbial enzymes is limited, and, today, there are only a handful of known bacterial phyla encoding active PET esterases (Fig. 1). PET-degrading enzymes belong to the classes of cutinases (EC3.1.1.74), lipases (EC3.1.1.3), or carboxylesterases (EC3.1.1.1). Diene lactone hydrolases (often grouped into EC3.1.1.45 of carboxymethylenebutenolidases) are not commonly known to degrade PET. Therefore, PET40 is one of the few enzymes known that belongs to this enzyme class and can act on PET.

Here, we identified and partially characterized the novel promiscuous esterase PET40, derived from a biochar metagenome. A more detailed phylogenetic analysis indicated that PET40 was affiliated with the genus *Amycolatopsis* within the Actinobacteria phylum. This genus is well-known to involve species that degrade a wide range of aromatic substances and plant-based polymers. It contains microorganisms that are ubiquitous and frequently isolated from soil and sediment samples. Furthermore, bacteria from this genus are well-known for their secondary metabolite production [56]. The genus currently contains more than 70 species. Most genomes appear to have sizes of 10 Mbp and larger. The genus is relatively closely related to the *Streptomyces* [57–60]. PET40 homology can be found in a significant fraction (21 out of 68) of the *Amylocolatopsis* and also *Streptomyces* (104 out of 564) genomes. This implies that enzymes with activity on PET are probably occurring more frequently than previously assumed.

PET40 appears to be a secreted enzyme, as it carries an N-terminal secretion signal, implying that the enzyme is probably released into the surrounding environment and can act on its substrates. Since it is well-known that some esterases are highly promiscuous enzymes being able to convert a large number of diverse substrates, it can be assumed that PET is not the primary substrate of PET40, as the polymer is present only relatively recent in nature next to much more favorable carbon sources and, especially, as turnover rates of PET40 are low compared with enzymes, whose primary substrate is PET, such as *Is*PETase. Promiscuous enzymes such as PET40 can turn over a broad range of substrates probably because of an exposed active site, a certain cavity volume-to-surface ratio [30] and certain structural rigidity characteristics [31]. Substrates that do not fit well into the active or binding site are turned over with lower rates than those substrates that fit best [30,31,61,62].

The activity of PET40 on PET was shown through the release of the degradation product TPA. In 200 µL reaction volume, it released 50.41 ± 10.21 µM of monomeric PET degradation products in a 72-h time period at 40 °C. Comparing activities of PET-active enzymes is generally difficult, as in most studies, different types of PET substrates with different degrees of crystallinity and distinct assay conditions have been used. To partly overcome this problem, we cloned and expressed the recombinant IsPETase and LCC and compared their activities with PET40 at suitable temperatures under otherwise identical assay conditions. Here, even though PET40 is less active than IsPETase and LCC, it still exhibited a distinct degradation activity on PET (Table 2). The observation that PET40 is catalytically active on PET implies a wider

Fig. 8. Docking poses for β-lactam antibiotics in PET40 have a similar geometry as in a crystallographically determined serine β-lactamase/β-lactam antibiotics complex. (A) Distance (*d*) and angle (α) between the protein and the substrate measured for the docking solutions. The structure shows the binding pose for the enzyme-substrate complex of a serine β-lactamase from *Mycobacterium tuberculosis* (PDB ID: 3NY4). Structures were generated using PYMOL [54]. (B) Dispersion plots showing the pairs of distance-angle values calculated for each docking solution of an antibiotic substrate in PET40. The color scale shows the docking score of the pose. The red dashed lines show the values observed in the crystal structure (PDB ID: 3NY4). Only imipenem yields no solution with similar geometry to the crystal complex.

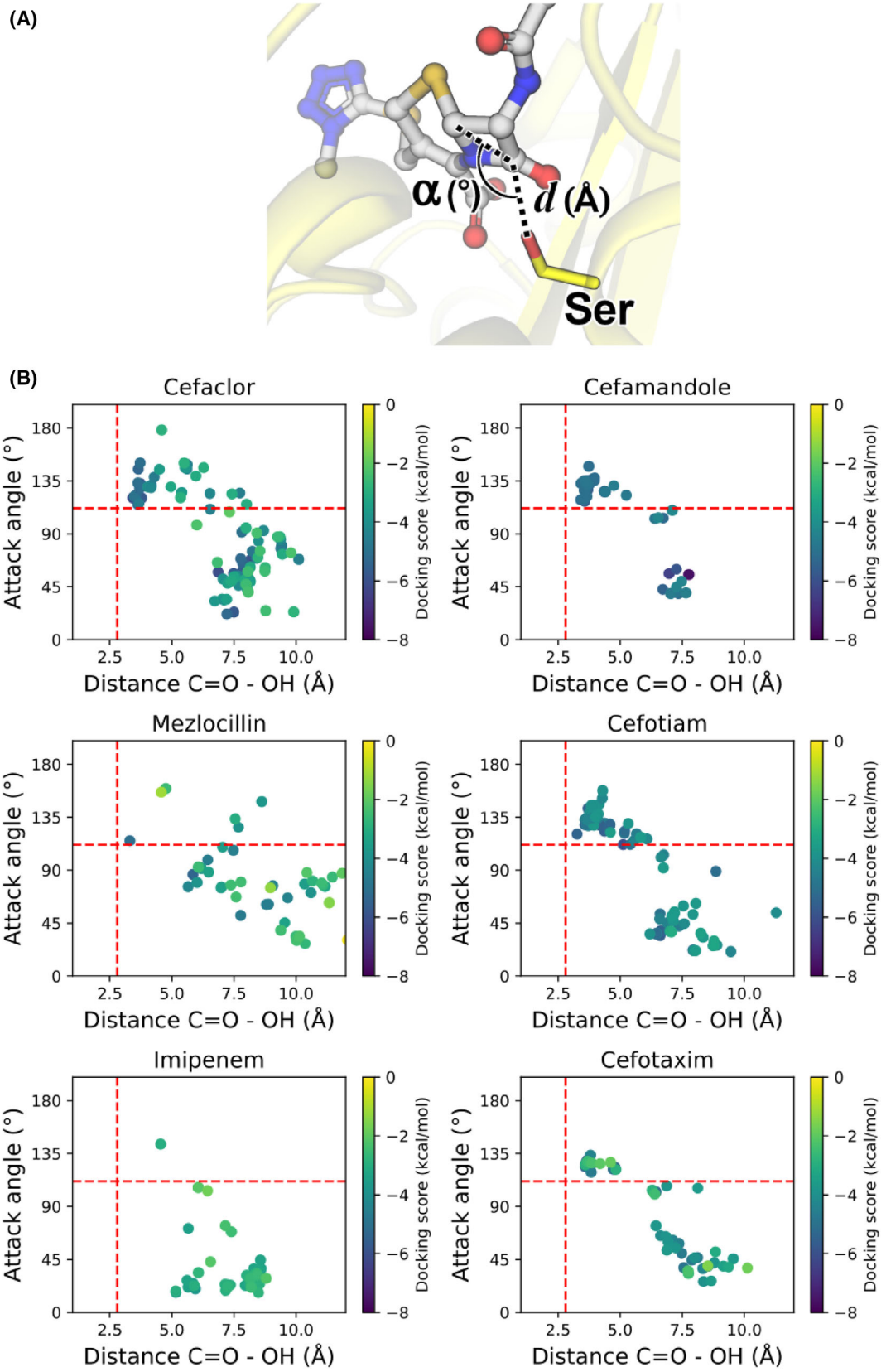

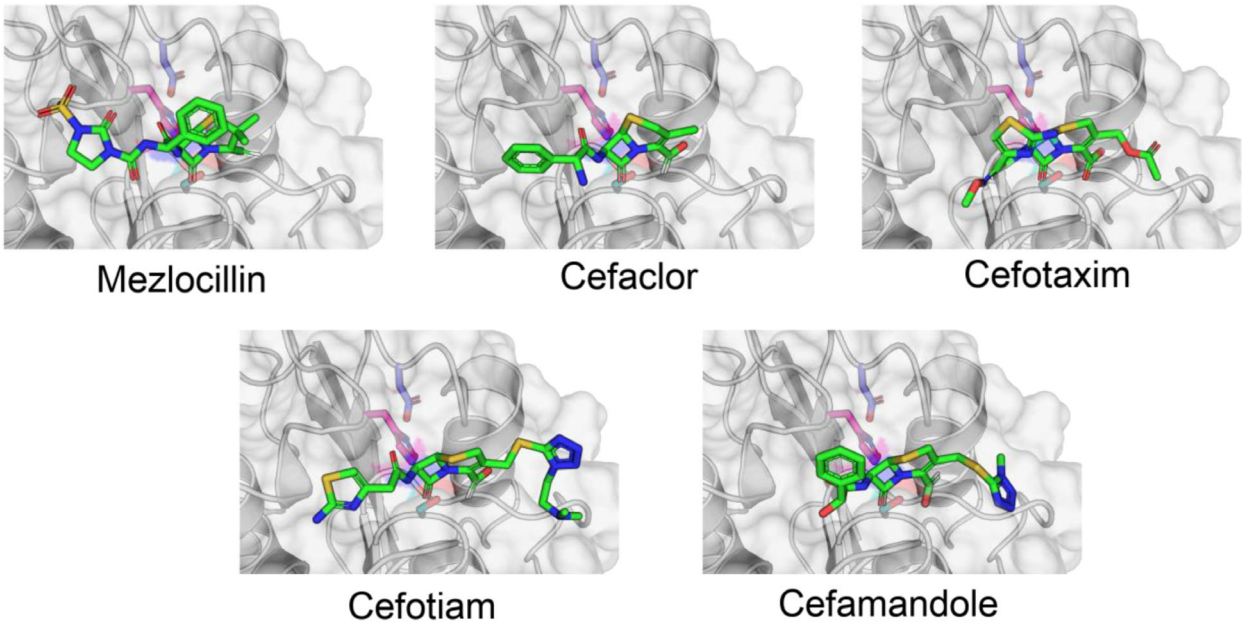

Fig. 9. Predicted binding poses for β-lactam antibiotics. The binding pose with the angle and distance that most closely resembles the crystal structure is shown for each antibiotic. The catalytic triad Ser-His-Asp is highlighted in cyan, purple, and violet, respectively. Structures were generated using PYMOL [54].

role of homologous enzymes in the degradation of this plastic, especially micro- and nanoparticles in nature. Particles reduced in size have an increased surface-to-volume ratio so that they can be better attacked by an enzyme. Therefore, the enzyme and its homologs may in fact play a heretofore unknown role in PET micro- and nanoparticle degradation This hypothesis is supported by our observation that homologs of PET degrading enzymes can be found on a global level, covering a wide range of climate zones, in a large fraction of the genomes of *Amycolatopsis* and *Streptomyces*. Both these bacterial genera are ubiquitous soil and marine organisms.

In summary, our biochemical data significantly extend the knowledge of promiscuous esterases with activity on PET derived from Gram-positive bacteria and provides PET40 as a novel promising and versatile candidate for further investigation and optimization. Within this framework, further possible substrates of the enzyme could be identified yielding more conceivable applications or present activities could be enhanced through alteration of the wildtype enzyme. Here, it could especially be of interest to elucidate the possible increase of the enzyme's activity on PET, for example through an amino acid exchange from Phe-Met-Trp to Tyr-Met-Trp in the substrate binding site. Furthermore, the data already presented here will help to advance our understanding on the evolution of genes encoding PET-active enzymes within the Gram-positive bacteria. Our research contributes to knowledge on the possible decomposition of marine and terrestrial PET litter and enables the development of an expanded phylogenetic framework for identifying the diversity of putative PETases in diverse microbial groups on a global scale.

Materials and methods

Bacterial strains, plasmids, and primers

Bacterial strains, plasmids, and primers employed in this study are listed in Table 5. *E. coli* clones were grown in LB medium (1% tryptone/peptone, 0.5% yeast extract, 1% NaCl) supplemented with appropriate antibiotics (25 $\mu g \cdot mL^{-1}$ kanamycin, or 100 $\mu g \cdot mL^{-1}$ ampicillin) at 37 °C for 18 h, if not indicated otherwise.

Databases used in this study and bioinformatic analysis

Nucleotide and amino acid sequences of the putative and confirmed PETases were acquired from databases integrated into the NCBI (https://www.ncbi.nlm.nih.gov/), UniProt (http://www.uniprot.org/) and IMG (JGI, http://jgi.doe.gov/) servers [63–65].

Sequence comparisons to other sequences deposited in the NCBI databases were conducted using the BLAST alignment tools [66]. The profile HMM search [33] was carried out using the HMMER (http://hmmer.org) webpage and a

Table 5. Bacterial strains and plasmids used in this work.

	Properties	Reference/source
Strain		
Escherichia coli DH5α	*supE*44 Δ*lacU*169 (Φ80 lac*Z* ΔM15) *hsdR*17 *recA*1 *endA*1 *gyrA*96 *thi*-1 *relA*1	Invitrogen (Karlsruhe, Germany)
E. coli BL21 (DE3)	F^-, *ompT*, *hsdS* B (r_B^- m_B^-) *gal*, *dcm*, λDE3	Novagen/Merck (Darmstadt, Germany)
E. coli SHuffle® T7	*huA*2 *lacZ*::T7 gene1 [lon] *ompT ahpC gal* λatt::pNEB3-r1-cDsbC (SpecR, lacIq) Δ*trxB sulA*11 R(mcr-73::miniTn10--TetS)2 [dcm] R(zgb-210::Tn10 --TetS) *endA*1 Δ*gor* Δ(*mcrC-mrr*)114::IS10	NEB (Frankfurt am Main, Germany)
Vector		
pET21a(+)	Expression vector, *lacI*, Amp^R, T7-*lac*- promoter, C-terminal His_6-tag coding sequence	Novagen/Merck (Darmstadt, Germany)
pET21a(+)::PET40	837 bp insert in pET21a(+) coding for PET40	This work
pET21a(+)::PET40_S178A	837 bp insert in pET21a(+) coding for PET40_S178A	This work
pET21a(+)::LCC	786 bp insert in pET21a(+) coding for LCC	This work, acc. to Sulaiman *et al.* [15]
pMAL-p4x::IsPETase	795 bp insert in pMAL-p4x coding for the wildtype *Is*PETase from *Ideonella sakaiensis* fused to a maltose binding protein for purification	Lab of Birte Hoecker, Univ. Bayreuth, acc. to Yoshida *et al.* [9]

local version of the software (v3.1b2) [67] with downloaded datasets. Structural information on LCC (PDB 4EB0) and IsPETase (PDB 6EQE) was retrieved from the RCSB-PDB database [68].

The DNA sequence data were processed and analyzed using CHROMASPRO 2.1.8 (Technelysium, Brisbane, Qld, Australia) and SNAPGENE (GSL Biotech LLC, San Diego, CA, USA). The amino acid sequence alignment was constructed employing structural alignments with T-COFFEE [13]. Overall, the amino acid sequences of 23 enzymes were included in this alignment. The phylogenetic tree was constructed by Maximum Likelihood method using MEGAX [14] using 1000 bootstraps. GenBank entries of the sequences used are listed in Table 1 or were retrieved from the PAZy database (www.pazy.eu; [8]). UHPLC profiles were plotted and edited using software MATLAB version R2021a (The MathWorks, Inc., Natick, MA, USA).

Heterologous production of PET40 in *E. coli* BL21 (DE3)

The putative PET-active enzyme PET40 was found in a metagenomic dataset. For this, the gene sequences were optimized for expression in *E. coli* and synthesized into pET21a(+) vector at Biomatik (Wilmington, DE, USA). The resulting construct was sequenced at Eurofins (Ebersberg, Germany) and verified for correctness by comparing to the original sequences. Chemically competent *E. coli* BL21 (DE3) were used for heterologous expression of the predicted PETase gene. Cultures carrying the expression plasmid were grown aerobically in auto-induction medium (ZYM-5052) [69] containing 100 $\mu g \cdot mL^{-1}$ ampicillin for pET21a(+) at 37 °C until they reached an optical density (OD_{600}) of 1.0. Proteins were produced afterwards at 22 °C for 16–20 h. Cells were harvested and lysed with pressure using a French press. From this lysate, recombinant PET40 was purified using nickel-ion affinity chromatography employing Ni-NTA agarose (Macherey-Nagel, Düren, Germany). The purified protein was analyzed by SDS/PAGE. Finally, the elution buffer was exchanged against 0.1 mM potassium phosphate buffer (pH 8.0) using a 10 kDa Amicon Tube (GE Health Care, Solingen, Germany).

PET degradation assay measured by UHPLC

To assay enzymatic PET hydrolysis, 5 mg of PET powder (Goodfellow GmbH, Bad Nauheim, Germany) were added to 1.5-mL Eppendorf tubes with 20 µg of enzyme in 200 µL of 100 mM potassium phosphate buffer at pH 8.0. Incubation was carried out under continuous shaking and at 400 r.p.m. in 1.5-mL microcentrifuge tubes. The incubation was made at PET40's optimal temperature of 40 °C if not stated otherwise.

The analysis of the degradation products was performed using an UltiMate™ 3000 UHPLC system (Thermo Scientific, Waltham, MA, USA) employing a Triart C18 column (YMC Europe GmbH, Dinslaken, Germany) and with a dimension of 100 × 2.0 mm containing particles with 1.9 µm diameter. Isocratic elution was made by using a mobile phase consisting of 20 : 80 (v/v) acetonitrile and water (acidified with 0.1% v/v trifluoroacetic acid) at a flowrate of 0.4 $mL \cdot min^{-1}$. All UHPLC samples were prepared by mixing 50 µL of incubation supernatant with 200 µL acetonitrile (acidified with 1% vol trifluoroacetic acid), followed by a centrifugation at 10 000 ***g*** for 3 min. Following this, 200 µL of the supernatant were transferred into 600 µL of water and 15 µL of sample were injected per measurement. The detection of breakdown products

was made at 254 nm with a VWD-3400 detector from Thermo Scientific. The quantification of peak areas was performed using the data analysis software supplied with the COMPASS HYSTAR software package from Bruker (Billerica, MA, USA).

Polyester polyurethane degradation assay with Impranil® DLN and phenol red

Impranil® DLN (Covestro AG, Leverkusen, Germany) was used as a model substrate for screening activity on an ester-based polyurethane. The assay was performed as previously described [30] with minor modifications. For sample preparation, 10 µL Impranil® DLN was added to a 96-well plate filled with 235 µL of *N*-(2-hydroxyethyl)piperazine-*N*′-3-propanesulfonic acid) (EPPS) buffer containing phenol red (0.5 mM final concentration) as a pH indicator. After adding 5 µL of purified protein (1 mg·mL^{-1}), the reaction was measured continuously at 550 nm during incubation at 40 °C in a microplate reader (BioTek Instruments Inc., Winooski, VT, USA) for 40 min. The reaction was assayed in triplicate per plate. Neither the actual structure of Impranil® DLN nor the degradation products are known. Therefore, in order to quantify the release of protons, a standard curve with acetic acid was employed.

Biochemical characterization of PET40 using *p*NP-esters

For activity tests, PET40 was assayed using purified recombinant protein. Unless otherwise indicated, a total amount of 0.25 µg of the enzyme was added to a substrate solution. The substrate solution contained 190 µL of 0.1 M potassium phosphate with a defined pH between 7 and 8 and 10 µL of 0.1 mM *p*NP-substrate dissolved in isopropanol. Samples were incubated for 10 min, and the assay was stopped by adding 200 mM of Na_2CO_3. After this, the samples were centrifuged at 18 000 ***g*** for 3 min and at 4 °C. The *p*NP-esters with chain lengths of C4, C6, C8, C10, C12, C14, C16 and C18 were tested as substrates. For the identification of the optimal temperature, the samples were incubated at different temperatures ranging between 4 °C and 90 °C for a 10-min time period. Following the incubation at the defined temperatures, release of the yellow *p*NP-OH was measured at 405 nm in a plate reader (BioTek Instruments Inc.). All samples were measured at least in triplicate. The influence of pH on the activity of each enzyme was measured in either citrate phosphate (pH 3.0, 4.0 and 5.0), or potassium phosphate (pH 6.0, 7.0 and 8.0) and/or in carbonate bicarbonate buffer (pH 9.2 and 10.2). The influence of cofactors, solvents, detergents, and inhibitors on PET40 was assayed at different concentration levels. The possible cofactors Ca^{2+}, Co^{2+}, Cu^{2+}, Fe^{3+}, Mg^{2+}, Mn^{2+}, Ni^{2+}, and Zn^{2+} were assayed at a concentration of 1 and 10 mM. Detergent stability was tested using a concentration of 1% and 5% of SDS (w/v), 1% and 5% of Triton X-100 and Tween 80 (v/v) in the test, respectively. Possible inhibitory effects of EDTA, DTT, and PMSF were assayed at 1 and 10 mM concentrations. The residual PET40 activity was determined after 10-min incubation at the optimal temperature of 40 °C with *p*NP-hexanoate (-C8) and at the optimal pH of pH8. Activity of PET40 after incubation with possible different cofactors detergents and solvents was assayed after 1 h of incubation in the presence of these substances.

Lactonase assay

The lactonase activity of PET 40 was investigated by performing a phenol red-assay according to Perez-Garcia *et al.* [49]. As substrates, δ-dodecalactone, γ-dodecalactone, γ-caprolactone and δ-octalactone (Sigma-Aldrich, Munich, Germany) were chosen, which release protons upon hydrolysis resulting in a pH shift. 100 mg·mL^{-1} stock solutions of the lactones were mixed with dimethyl sulfoxide and stored at −20 °C. 8 µL substrate was incubated with 5 µL protein (1 mg·mL^{-1}) and 5 mM EPPS buffer including phenol red with a final concentration of 0.45 mM in a 250 µL reaction volume. At 40 °C, the enzymatic activity was measured at 550 nm every 15 min. The samples were measured in triplicates, including additional negative controls with enzyme-free buffer. The enzymatic activity, calculated in units (U)·mg^{-1}, was determined according to the Lambert–Beer law using the reported extinction coefficient of phenol red (8450 M^{-1}·cm^{-1}) [30] together with the highest determined initial reduction in extinction values throughout the first hour of measurement. One unit is defined as the amount of protein needed to transform 1 µmol of substrate in 1 min under the abovementioned assay conditions.

Disk-diffusion antibiotic sensitivity test

To test the lactamase activity of PET40, a disk diffusion test was conducted with antibiotic disks containing effective antibiotic concentrations. The disks containing mezlocillin 30 µg (MEZ 30), imipenem 10 µg (IPM 10), cefaclor 30 µg (CEC 30), cefamandole 30 µg (MA 30), cefotiam 30 µg (CFT 30), and cefotaxim 30 µg (CTX 30) were incubated with 20 µL of potassium buffer pH 8 containing 1 mg·mL^{-1} of the purified recombinant protein. The disks were incubated for over 17 h at 40 °C. As a negative control, disks were incubated with the same volume of enzyme-free buffer. Afterwards, the antibiotic disks were laid on LB-agar plates on which susceptible *E. coli* DH5α cells had been spread. The agar plates were incubated overnight at 37 °C. The clear zone formation around the disks indicates the ZOI by various β-lactam antibiotics. The reduction of ZOI was calculated in comparison to the negative controls (Fig. 5).

Binding mode prediction via molecular docking

We applied the AlphaFold2-based workflow of ColabFold [70] to generate the 3D structural model of the PET40 wild-type. A single model was generated with 10 prediction cycles (--num_recycles) and structurally refined by running a relaxation with AMBER (--amber). The modeling was made before the crystal structure of PET40_S178A was solved. The structural model and the crystal structure have an RMSD of 1.26 overall and 0.44 in the binding site. All docked ligands were generated from their respective SMILES code [71] using OPENBABEL v.2.4.1 [72]. For the docking, we considered the following substrates: mono(2-hydroxyethyl) terephthalate (MHET), bis(2-hydroxyethyl) terephthalate (BHET), PET trimer (PET_3), methyl hexanoate (MH), polycaprolactone trimer (PCL_3), propane-1,2,3-triyl tributanoate (tributyrin, TBT), 4-nitrophenyl decanoate (*p*NP-C10), and 4-nitrophenyl dodecanoate (*p*NP-C12).

The substrates were docked into the catalytic site of the PET40 wild-type utilizing a combination of AutoDock3 [46] as a docking engine and DrugScore^{2018} [47,48] as an objective function [50]. Docking grids with a grid spacing of 0.5 Å were generated with DrugScore^{2018} using converged pair potentials for all atom pairs. The position and dimension of the docking grid were automatically calculated by DrugScore^{2018} using the largest substrate (PET_3) manually placed into the binding site as a reference. Accounting for a margin of 6 Å in every direction, the final docking grid has box dimensions of approximately 32 Å × 46 Å × 30 Å and is centered in the active site of PET40. We adapted an established procedure [47] to account for the high number of rotational degrees of freedom of the oligomeric substrates. The docking protocol considered 100 independent runs for each ligand using an initial population size of 100 individuals, a maximum number of 10^5 generations, a maximum number of 5.0×10^7 energy evaluations, a mutation rate of 0.02, a crossover rate of 0.8, and an elitism value of 1. All 100 docking solutions were clustered based on structural similarity (RMSD cut-off < 2 Å), yielding a few distinct binding modes. Of these, the best-scored pose was considered the final solution except for *p*NP-C10 and *p*NP-C12, for which the pose from the largest cluster was taken (Results section). The Lamarckian genetic algorithm was chosen for sampling in all approaches.

The distance between the reactive carbonyl carbon atom of the docked substrates and the hydroxy group oxygen of PET40_S178 was measured using PYTRAJ [73], a PYTHON package binding to the CPPTRAJ program [74].

The antibiotic compounds (mezlocillin, cefaclor, cefotaxim, cefotiam, cefamandole, and imipenem) were prepared for docking using LIGPREP [75]. Protonation states were assigned with EpiK at pH 7. Ligands were docked onto the same protein structure, using a grid of 35 Å in every direction, centered between the catalytic residues S178 and H256. Docking was carried out using GLIDE [76] in standard precision mode, using OPLS_2005 as the force field and generating 50 poses per ligand. The distance between the serine hydroxyl and the carbonyl carbon as well as the angle between the serine hydroxyl, the carbonyl carbon, and the carbon opposite the carbonyl carbon in the lactam ring were calculated using PYMOL'S PYTHON API. Reference values of distance and angle were calculated from the crystal structure of a serine β-lactamase from *Mycobacterium tuberculosis* bound to cefamandole (PDB ID 3NY4).

Site-directed mutagenesis to generate the inactive mutant PET40_S178A

Trying to obtain a cocrystal structure of PET40 with a substrate, an inactive mutant of PET40 was generated in which the active site Ser178 was replaced by Ala. Therefore, the primer pair PET40/S178ala_for (5′-GCTTAGGAGTTG TGGGCCAT**GCG**ATGGGTGGTGG-3′) and PET40/S178ala_rev (5′-GTGCCACCACCACCCAT**CGC**ATGG CCCACAAC-3′) were used on PET40::pET21a(+) as a template in a three-step gradient-PCR (T_{ann} = 55–61 °C, fragment size: 6138 bp), resulting in an amplification of the whole vector including the mutagenized insert. After PCR cleanup, the DNA mixture was digested with 1 µL *Dpn*I overnight at 37 °C to cleave all methylated template DNA. The following day, the restriction enzyme was inactivated at 80 °C for 20 min and the reaction transformed into *E. coli* DH5α. Colonies were spread on LB agar plates containing 100 $\mu g \cdot mL^{-1}$ ampicillin and incubated at 37 °C overnight. The isolated plasmids were sequenced using the primers pET_19_21_24_for (5′-ATATAGGCGCCAGCAA CC-3′) and T7 Terminator: (5′-GCTAGTTATTGCTCA GCGG-3′) and the resulting sequence was checked for correctness.

Crystallization, data collection, data reduction, structure determination, refinement, and final model analysis

PET40_S178A was crystallized by sitting-drop vapor diffusion at 12 °C at a concentration of 11 $mg \cdot mL^{-1}$ in 100 mM potassium phosphate buffer pH 7.0. 0.1 µL of this solution was mixed with 0.1 µL reservoir solution consisting of 0.2 M magnesium chloride hexahydrate, 10% (v/v) EG, 0.1 M 4-(2-hydroxyethyl)piperazine-1-ethanesulfonic acid (HEPES) pH 7.5, 15% (v/v) polyethylene glycol (PEG) Smear medium, 5% v/v 2-propanol. This drop was equilibrated against the reservoir solution and crystals formed after 4 weeks. Crystallization drops were overlaid with mineral oil, and the crystals were dragged through it for cryoprotection, and flash-frozen in liquid nitrogen.

Diffraction data were collected at 100 K at beamline ID23-1 (ESRF, Grenoble, France) using a 0.8856 Å wavelength.

Table 6. Data collection and refinement statistics for the PET40 mutant S178A. Values in parenthesis refer to the high-resolution shell.

PET40 S178A	
PDB ID	8A2C
Data collection	
Wavelength (Å)	0.8856
Space group	$P2_1$
Unit cell parameters	
a, *b*, *c* (Å)	46.0, 110.0, 47.9
α, β, γ (°)	90.00, 95.74, 90.00
Resolution (Å)	110.00–1.60 (1.63–1.60)
Number of unique reflections	61 003 (2989)
R_{merge}	0.075 (0.741)
R_{meas}	0.091 (0.895)
R_{pim}	0.051 (0.495)
$<I/\sigma(I)>$	7.3 (1.5)
$CC^{1/2}$	0.997 (0.613)
Completeness (%)	97.7 (97.4)
Multiplicity	3.0 (3.1)
Refinement	
Resolution (Å)	31.51–1.60
Number of reflections	60 973
R_{work}/R_{free} (%)	14.59/17.90
r.m.s. deviations	
Bond length (Å)	0.011
Bond angles (°)	1.140
Ramachandran plot	
Favored (%)	98.29
Allowed (%)	1.71
Outliers (%)	0

Data reduction was performed using the program package XDS [77] and AIMLESS [78] from the CCP4 suite [79]. The structure was solved via molecular replacement with PHASER [80] using an AlphaFold model as a search model. The initial model was refined through alternating cycles of manual model building in COOT [81,82] and automatic refinement using PHENIX [83] version 1.19.2_4158. Data collection and refinement statistics are reported in Table 6. The structure assembly was analyzed using PISA [44].

Acknowledgments

This work was in part supported by the BMBF within the programs MetagenLig (031B0571B), LipoBiocat (031B0837A, 031B0837B), and PlastiSea (031B867B) as well as by the EU commission's Horizon 2020 research and innovation program FuturEnzymes under grant agreement no. 101000327. The plasmid containing the IsPETase gene was kindly provided by Birte Höcker at the University of Bayreuth. We are grateful for computational support and infrastructure provided by the "Zentrum für Informations- und Medientechnologie" (ZIM) at the Heinrich Heine University Düsseldorf, and the computing time provided by the John von Neumann Institute for Computing (NIC) to HG on the supercomputer JUWELS at Jülich Supercomputing Centre (JSC) (user ID: VSK33, lipases). The Center for Structural Studies is funded by the Deutsche Forschungsgemeinschaft (DFG Grant number 417919780 and INST 208/740-1 FUGG) to SHJS. We would like to thank Rebecka Molitor and Stephan Thies from the Institute of Molecular Enzyme Technology at the Heinrich Heine university Düsseldorf for NanoDSF measurements. Open Access funding enabled and organized by Projekt DEAL.

Conflict of interest

The authors declare no conflict of interest.

Author contributions

WRS, JC, and PP-G designed the study, coordinated manuscript writing and bioassays. HZ, and KP contributed to planning, assay conduction, writing, and data collection. RFD was involved in writing, protein expression, and UHPLC analysis. MG contributed to activity assays. HZ, JC, and PP-G were involved in enzyme structural work, bioinformatics, and initial phylogenetic analyses. EC, VA, and SHJS conducted crystallization and structure determination. JD, PAC, CP, and HG performed molecular docking analyses. CS was involved in planning and corrections. All authors contributed to manuscript writing and editing.

Peer review

The peer review history for this article is available at https://www.webofscience.com/api/gateway/wos/peer-review/10.1111/febs.16924.

Data availability statement

DNA sequences of the identified and in part functionally verified PET40 esterase is listed in (Table 2) and a new GenBank entry has been deposited with the codon optimized protein sequence of PET40 under the accession number ON332566. Coordinates and structure factors of the X-ray crystal structure of PET40 S178A were deposited to the Protein Data Bank with accession number 8A2C.

References

1 Brandon JA, Jones W & Ohman MD (2019) Multidecadal increase in plastic particles in coastal ocean sediments. *Sci Adv* **5**, eaax0587.

2 Geyer R, Jambeck JR & Law KL (2017) Production, use, and fate of all plastics ever made. *Sci Adv* **3**, e1700782.
3 Danso D, Chow J & Streit WR (2019) Plastics: microbial degradation, environmental and biotechnological perspectives. *Appl Environ Microbiol* **85**, e01095-19.
4 Wei R & Zimmermann W (2017) Microbial enzymes for the recycling of recalcitrant petroleum-based plastics: how far are we? *J Microbial Biotechnol* **10**, 1308–1322.
5 Kawai F, Kawabata T & Oda M (2019) Current knowledge on enzymatic PET degradation and its possible application to waste stream management and other fields. *Appl Microbiol Biotechnol* **103**, 4253–4268.
6 Chow J, Perez-Garcia P, Dierkes R & Streit WR (2022) Microbial enzymes will offer limited solutions to the global plastic pollution crisis. *J Microbial Biotechnol* **16**, 195–217.
7 Tournier V, Duquesne S, Guillamot F, Cramail H, Taton D, Marty A & André I (2023) Enzymes' power for plastics degradation. *Chem Rev* **123**, 5612–5701.
8 Buchholz PCF, Feuerriegel G, Zhang H, Perez-Garcia P, Nover L-L, Chow J, Streit WR & Pleiss J (2022) Plastics degradation by hydrolytic enzymes: the plastics-active enzymes database—PAZy. *Proteins* **90**, 1443–1456.
9 Yoshida S, Hiraga K, Takehana T, Taniguchi I, Yamaji H, Maeda Y, Toyohara K, Miyamoto K, Kimura Y & Oda K (2016) A bacterium that degrades and assimilates poly(ethylene terephthalate). *Science* **351**, 1196–1199.
10 Wei R, von Haugwitz G, Pfaff L, Mican J, Badenhorst CPS, Liu W, Weber G, Austin HP, Bednar D, Damborsky J *et al.* (2022) Mechanism-based design of efficient PET hydrolases. *ACS Catal* **12**, 3382–3396.
11 Wang YZ, Zhou Y & Zylstra GJ (1995) Molecular analysis of isophthalate and terephthalate degradation by *Comamonas testosteroni* YZW-D. *Environ Health Perspect* **103** (Suppl 5), 9–12.
12 Choi KY, Kim D, Sul WJ, Chae J-C, Zylstra GJ, Kim YM & Kim E (2005) Molecular and biochemical analysis of phthalate and terephthalate degradation by *Rhodococcus* sp. strain DK17. *FEMS Microbiol Lett* **252**, 207–213.
13 Notredame C, Higgins DG & Heringa J (2000) T-coffee: a novel method for fast and accurate multiple sequence alignment. *J Mol Biol* **302**, 205–217.
14 Kumar S, Stecher G, Li M, Knyaz C & Tamura K (2018) MEGA X: molecular evolutionary genetics analysis across computing platforms. *Mol Biol Evol* **35**, 1547–1549.
15 Sulaiman S, Yamato S, Kanaya E, Kim J-J, Koga Y, Takano K & Kanaya S (2012) Isolation of a novel cutinase homolog with polyethylene terephthalate-degrading activity from leaf-branch compost by using a metagenomic approach. *Appl Environ Microbiol* **78**, 1556–1562.
16 Ribitsch D, Herrero Acero E, Greimel K, Dellacher A, Zitzenbacher S, Marold A, Rodriguez RD, Steinkellner G, Gruber K, Schwab H *et al.* (2012) A new esterase from *Thermobifida halotolerans* hydrolyses polyethylene terephthalate (PET) and polylactic acid (PLA). *Polymers* **4**, 617–629.
17 Roth C, Wei R, Oeser T, Then J, Follner C, Zimmermann W & Strater N (2014) Structural and functional studies on a thermostable polyethylene terephthalate degrading hydrolase from *Thermobifida fusca*. *Appl Microbiol Biotechnol* **98**, 7815–7823.
18 Wei R, Oeser T, Then J, Kuhn N, Barth M, Schmidt J & Zimmermann W (2014) Functional characterization and structural modeling of synthetic polyester-degrading hydrolases from *Thermomonospora curvata*. *AMB Express* **4**, 44.
19 Kawai F, Oda M, Tamashiro T, Waku T, Tanaka N, Yamamoto M, Mizushima H, Miyakawa T & Tanokura M (2014) A novel Ca(2)(+)-activated, thermostabilized polyesterase capable of hydrolyzing polyethylene terephthalate from *Saccharomonospora viridis* AHK190. *Appl Microbiol Biotechnol* **98**, 10053–10064.
20 Chertkov O, Sikorski J, Nolan M, Lapidus A, Lucas S, Del Rio TG, Tice H, Cheng J-F, Goodwin L & Pitluck S (2011) Complete genome sequence of *Thermomonospora curvata* type strain (B9 T). *Stand Genomic Sci* **4**, 13–22.
21 Müller R, Schrader H, Profe J, Dresler K & Deckwer W (2005) Enzymatic degradation of poly (ethylene terephthalate): rapid hydrolyse using a hydrolase from *T. fusca*. *Macromol Rapid Commun* **26**, 1400–1405.
22 Herrero Acero E, Ribitsch D, Steinkellner G, Gruber K, Greimel K, Eiteljoerg I, Trotscha E, Wei R, Zimmermann W, Zinn M *et al.* (2011) Enzymatic surface hydrolysis of PET: effect of structural diversity on kinetic properties of cutinases from *Thermobifida*. *Macromolecules* **44**, 4632–4640.
23 Bollinger A, Thies S, Katzke N & Jaeger KE (2020) The biotechnological potential of marine bacteria in the novel lineage of *Pseudomonas pertucinogena*. *Microb Biotechnol* **13**, 19–31.
24 Bollinger A, Thies S, Knieps-Grunhagen E, Gertzen C, Kobus S, Hoppner A, Ferrer M, Gohlke H, Smits SHJ & Jaeger KE (2020) A novel polyester hydrolase from the marine bacterium *Pseudomonas aestusnigri* – structural and functional insights. *Front Microbiol* **11**, 114.
25 Haernvall K, Zitzenbacher S, Yamamoto M, Schick MB, Ribitsch D & Guebitz GM (2017) A new arylesterase from *Pseudomonas pseudoalcaligenes* can hydrolyze ionic phthalic polyesters. *J Biotechnol* **257**, 70–77.

26 Zhang H, Perez-Garcia P, Dierkes RF, Applegate V, Schumacher J, Chibani CM, Sternagel S, Preuss L, Weigert S, Schmeisser C *et al.* (2022) The bacteroidetes *Aequorivita* sp. and *Kaistella jeonii produce* promiscuous esterases with PET-hydrolyzing activity. *Front Microbiol* **12**, 803896.

27 Joo S, Cho IJ, Seo H, Son HF, Sagong HY, Shin TJ, Choi SY, Lee SY & Kim KJ (2018) Structural insight into molecular mechanism of poly(ethylene terephthalate) degradation. *Nat Commun* **9**, 382.

28 Kawai F (2021) The current state of research on PET hydrolyzing enzymes available for biorecycling. *Catalysts* **11**, 206.

29 Carniel A, Valoni É, Nicomedes J, Gomes AC & Castro AM (2017) Lipase from *Candida antarctica* (CALB) and cutinase from *Humicola insolens* act synergistically for PET hydrolysis to terephthalic acid. *Process Biochem* **59**, 84–90.

30 Martinez-Martinez M, Coscolin C, Santiago G, Chow J, Stogios PJ, Bargiela R, Gertler C, Navarro-Fernandez J, Bollinger A, Thies S *et al.* (2018) Determinants and prediction of esterase substrate promiscuity patterns. *ACS Chem Biol* **13**, 225–234.

31 Nutschel C, Coscolín C, David B, Mulnaes D, Ferrer M, Jaeger K-E & Gohlke H (2021) Promiscuous esterases counterintuitively are less flexible than specific ones. *J Chem Inf Model* **61**, 2383–2395.

32 Danso D, Schmeisser C, Chow J, Zimmermann W, Wei R, Leggewie C, Li X, Hazen T & Streit WR (2018) New insights into the function and global distribution of polyethylene terephthalate (PET)-degrading bacteria and enzymes in marine and terrestrial metagenomes. *Appl Environ Microbiol* **84**, e02773-17.

33 Pérez-García P, Danso D, Zhang H, Chow J & Streit WR (2021) Exploring the global metagenome for plastic-degrading enzymes. *Methods Enzymol* **648**, 137–157.

34 Sonnendecker C, Oeser J, Richter PK, Hille P, Zhao Z, Fischer C, Lippold H, Blázquez-Sánchez P, Engelberger F & Ramírez-Sarmiento CA (2022) Low carbon footprint recycling of post-consumer PET plastic with a metagenomic polyester hydrolase. *ChemSusChem* **15**, e202101062.

35 Benson DA, Cavanaugh M, Clark K, Karsch-Mizrachi I, Lipman DJ, Ostell J & Sayers EW (2012) GenBank. *Nucleic Acids Res* **41**, D36–D42.

36 Chen I-MA, Chu K, Palaniappan K, Ratner A, Huang J, Huntemann M, Hajek P, Ritter S, Varghese N & Seshadri R (2021) The IMG/M data management and analysis system v. 6.0: new tools and advanced capabilities. *Nucleic Acids Res* **49**, D751–D763.

37 Ye J, Joseph SD, Ji M, Nielsen S, Mitchell DRG, Donne S, Horvat J, Wang J, Munroe P & Thomas T (2017) Chemolithotrophic processes in the bacterial communities on the surface of mineral-enriched biochars. *ISME J* **11**, 1087–1101.

38 Wei R, Oeser T & Zimmermann W (2014) Synthetic polyester-hydrolyzing enzymes from thermophilic actinomycetes. *Adv Appl Microbiol* **89**, 267–305.

39 Austin HP, Allen MD, Donohoe BS, Rorrer NA, Kearns FL, Silveira RL, Pollard BC, Dominick G, Duman R, El Omari K *et al.* (2018) Characterization and engineering of a plastic-degrading aromatic polyesterase. *Proc Natl Acad Sci USA* **115**, E4350–E4357.

40 Sulaiman S, You DJ, Kanaya E, Koga Y & Kanaya S (2014) Crystal structure and thermodynamic and kinetic stability of metagenome-derived LC-cutinase. *Biochemistry* **53**, 1858–1869.

41 Pettersen EF, Goddard TD, Huang CC, Couch GS, Greenblatt DM, Meng EC & Ferrin TE (2004) UCSF Chimera – a visualization system for exploratory research and analysis. *J Comput Chem* **25**, 1605–1612.

42 Teufel F, Armenteros JJA, Johansen AR, Gíslason MH, Pihl SI, Tsirigos KD, Winther O, Brunak S, von Heijne G & Nielsen H (2021) SignalP 6.0 achieves signal peptide prediction across all types using protein language models. *bioRxiv*. doi: 10.1101/2021.06.09.447770

43 Ollis DL, Cheah E, Cygler M, Dijkstra B, Frolow F, Franken SM, Harel M, Remington SJ, Silman I, Schrag J *et al.* (1992) The alpha/beta hydrolase fold. *Protein Eng* **5**, 197–211.

44 Krissinel E & Henrick K (2007) Inference of macromolecular assemblies from crystalline state. *J Mol Biol* **372**, 774–797.

45 Miyakawa T, Mizushima H, Ohtsuka J, Oda M, Kawai F & Tanokura M (2015) Structural basis for the Ca (2+)-enhanced thermostability and activity of PET-degrading cutinase-like enzyme from *Saccharomonospora viridis* AHK190. *Appl Microbiol Biotechnol* **99**, 4297–4307.

46 Morris GM, Goodsell DS, Halliday RS, Huey R, Hart WE, Belew RK & Olson AJ (1998) Automated docking using a Lamarckian genetic algorithm and an empirical binding free energy function. *J Comput Chem* **19**, 1639–1662.

47 Dittrich J, Schmidt D, Pfleger C & Gohlke H (2018) Converging a knowledge-based scoring function: DrugScore2018. *J Chem Inf Model* **59**, 509–521.

48 Gohlke H, Hendlich M & Klebe G (2000) Knowledge-based scoring function to predict protein-ligand interactions. *J Mol Biol* **295**, 337–356.

49 Perez-Garcia P, Kobus S, Gertzen CG, Hoeppner A, Holzscheck N, Strunk CH, Huber H, Jaeger K-E, Gohlke H & Kovacic F (2021) A promiscuous ancestral enzyme's structure unveils protein variable regions of the highly diverse metallo-β-lactamase family. *Commun Biol* **4**, 1–12.

50 Sotriffer CA, Gohlke H & Klebe G (2002) Docking into knowledge-based potential fields: a comparative evaluation of DrugScore. *J Med Chem* **45**, 1967–1970.

51 Mobley DL & Dill KA (2009) Binding of small-molecule ligands to proteins: "what you see" is not always "what you get". *Structure* **17**, 489–498.
52 Schauperl M, Czodrowski P, Fuchs JE, Huber RG, Waldner BJ, Podewitz M, Kramer C & Liedl KR (2017) Binding pose flip explained via enthalpic and entropic contributions. *J Chem Inf Model* **57**, 345–354.
53 Wienen-Schmidt B, Oebbeke M, Ngo K, Heine A & Klebe G (2021) Two methods, one goal: structural differences between cocrystallization and crystal soaking to discover ligand binding poses. *ChemMedChem* **16**, 292–300.
54 Schrödinger, LLC (2015) The PyMOL Molecular Graphics System, Version 2.0. Schrödinger, LLC, New York, NY.
55 Krüger DM, Jessen G & Gohlke H (2012) How good are state-of-the-art docking tools in predicting ligand binding modes in protein–protein interfaces? *J Chem Inf Model* **52**, 2807–2811.
56 Song Z, Xu T, Wang J, Hou Y, Liu C, Liu S & Wu S (2021) Secondary metabolites of the genus *Amycolatopsis*: structures, bioactivities and biosynthesis. *Molecules* **26**, 1884.
57 Nouioui I, Carro L, García-López M, Meier-Kolthoff JP, Woyke T, Kyrpides NC, Pukall R, Klenk H-P, Goodfellow M & Göker M (2018) Genome-based taxonomic classification of the phylum Actinobacteria. *Front Microbiol* **9**, 2007.
58 Xu L, Huang H, Wei W, Zhong Y, Tang B, Yuan H, Zhu L, Huang W, Ge M, Yang S *et al.* (2014) Complete genome sequence and comparative genomic analyses of the vancomycin-producing *Amycolatopsis orientalis*. *BMC Genomics* **15**, 363.
59 Adamek M, Alanjary M, Sales-Ortells H, Goodfellow M, Bull AT, Winkler A, Wibberg D, Kalinowski J & Ziemert N (2018) Comparative genomics reveals phylogenetic distribution patterns of secondary metabolites in *Amycolatopsis* species. *BMC Genomics* **19**, 426.
60 Chen S, Wu Q, Shen Q & Wang H (2016) Progress in understanding the genetic information and biosynthetic pathways behind *Amycolatopsis* antibiotics, with implications for the continued discovery of novel drugs. *Chembiochem* **17**, 119–128.
61 Hult K & Berglund P (2007) Enzyme promiscuity: mechanism and applications. *Trends Biotechnol* **25**, 231–238.
62 Leveson-Gower RB, Mayer C & Roelfes G (2019) The importance of catalytic promiscuity for enzyme design and evolution. *Nat Rev Chem* **3**, 687–705.
63 Coordinators NR (2017) Database resources of the National Center for Biotechnology Information. *Nucleic Acids Res* **45**, D12–D17.
64 The UniProt Consortium (2017) UniProt: the universal protein knowledgebase. *Nucleic Acids Res* **45**, D158–D169.
65 Markowitz VM, Chen IM, Palaniappan K, Chu K, Szeto E, Grechkin Y, Ratner A, Jacob B, Huang J, Williams P *et al.* (2012) IMG: the integrated microbial genomes database and comparative analysis system. *Nucleic Acids Res* **40**, D115–D122.
66 Agarwala R, Barrett T, Beck J, Benson DA, Bollin C, Bolton E, Bourexis D, Brister JR, Bryant SH, Lanese K *et al.* (2016) Database resources of the National Center for Biotechnology Information. *Nucleic Acids Res* **44**, D7–D19.
67 Mistry J, Finn RD, Eddy SR, Bateman A & Punta M (2013) Challenges in homology search: HMMER3 and convergent evolution of coiled-coil regions. *Nucleic Acids Res* **41**, e121.
68 Berman HM, Westbrook J, Feng Z, Gilliland G, Bhat TN, Weissig H, Shindyalov IN & Bourne PE (2000) The protein data bank. *Nucleic Acids Res* **28**, 235–242.
69 Studier FW (2005) Protein production by auto-induction in high density shaking cultures. *Protein Expr Purif* **41**, 207–234.
70 Mirdita M, Schütze K, Moriwaki Y, Heo L, Ovchinnikov S & Steinegger M (2022) ColabFold: making protein folding accessible to all. *Nat Methods* **19**, 679–682.
71 Weininger D (1988) SMILES, a chemical language and information system. 1. Introduction to methodology and encoding rules. *J Chem Inf Comput Sci* **28**, 31–36.
72 O'Boyle NM, Banck M, James CA, Morley C, Vandermeersch T & Hutchison GR (2011) Open babel: an open chemical toolbox. *J Chem* **3**, 1–14.
73 Nguyen H, Roe DR, Swails J & Case DA (2016) PYTRAJ: Interactive Data Analysis for Molecular Dynamics Simulations. Rutgers University, New Brunswick, NJ.
74 Roe DR & Cheatham TE III (2013) PTRAJ and CPPTRAJ: software for processing and analysis of molecular dynamics trajectory data. *J Chem Theor Comput* **9**, 3084–3095.
75 Schrödinger, LLC (2023) Schrödinger Release 2023-2: LigPrep. Schrödinger, LLC, New York, NY.
76 Schrödinger, LLC (2023) Schrödinger Release 2023-2: Glide. Schrödinger, LLC, New York, NY.
77 Kabsch W (2010) XDS. *Acta Crystallogr D* **66**, 125–132.
78 Evans PR & Murshudov GN (2013) How good are my data and what is the resolution? *Acta Crystallogr D* **69**, 1204–1214.
79 Winn MD, Ballard CC, Cowtan KD, Dodson EJ, Emsley P, Evans PR, Keegan RM, Krissinel EB, Leslie AG & McCoy A (2011) Overview of the CCP4 suite and current developments. *Acta Crystallogr D* **67**, 235–242.
80 McCoy AJ, Grosse-Kunstleve RW, Adams PD, Winn MD, Storoni LC & Read RJ (2007) Phaser crystallographic software. *J Appl Cryst* **40**, 658–674.

81 Emsley P & Cowtan K (2004) Coot: model-building tools for molecular graphics. *Acta Crystallogr D* **60**, 2126–2132.
82 Emsley P, Lohkamp B, Scott WG & Cowtan K (2010) Features and development of Coot. *Acta Crystallogr D* **66**, 486–501.
83 Liebschner D, Afonine PV, Baker ML, Bunkoczi G, Chen VB, Croll TI, Hintze B, Hung LW, Jain S, McCoy AJ *et al.* (2019) Macromolecular structure determination using X-rays, neutrons and electrons: recent developments in Phenix. *Acta Crystallogr D* **75**, 861–877.